HHS Public Access

Author manuscript

Cell Rep. Author manuscript; available in PMC 2024 September 13.

Published in final edited form as:

Cell Rep. 2024 July 23; 43(7): 114488. doi:10.1016/j.celrep.2024.114488.

Therapeutic targeting of immunometabolism reveals a critical reliance on hexokinase 2 dosage for microglial activation and Alzheimer's progression

Juan F. Codocedo[1,2], **Claudia Mera-Reina**[1,2], **Peter Bor-Chian Lin**[1], **Paul B. Fallen**[1,2], **Shweta S. Puntambekar**[1,3], **Brad T. Casali**[1,2], **Nur Jury-Garfe**[1,2], **Pablo Martinez**[1,2], **Cristian A. Lasagna-Reeves**[1,2], **Gary E. Landreth**[1,2,4,*]

[1]Stark Neurosciences Research Institute, Indiana University School of Medicine, Indianapolis, IN 46202, USA

[2]Department of Anatomy, Cell Biology and Physiology, Indiana University School of Medicine, Indianapolis, IN 46202, USA

[3]Department of Medical and Molecular Genetics, Indiana University School of Medicine, Indianapolis, IN 46202, USA

[4]Lead contact

SUMMARY

Neuroinflammation is a prominent feature of Alzheimer's disease (AD). Activated microglia undergo a reprogramming of cellular metabolism necessary to power their cellular activities during disease. Thus, selective targeting of microglial immunometabolism might be of therapeutic benefit for treating AD. In the AD brain, the levels of microglial hexokinase 2 (HK2), an enzyme that supports inflammatory responses by promoting glycolysis, are significantly increased. In addition, HK2 displays non-metabolic activities that extend its inflammatory role beyond glycolysis. The antagonism of HK2 affects microglial phenotypes and disease progression in a gene-dose-dependent manner. HK2 complete loss fails to improve pathology by exacerbating inflammation, while its haploinsufficiency reduces pathology in 5xFAD mice. We propose that the partial antagonism of HK2 is effective in slowing disease progression by modulating NF-κB signaling through its cytosolic target, IKBα. The complete loss of HK2 affects additional inflammatory mechanisms related to mitochondrial dysfunction.

In brief

*Correspondence: glandret@iu.edu.

AUTHOR CONTRIBUTIONS

J.F.C. and G.E.L. designed the experiments and wrote the manuscript. J.F.C. and C.M.-R. performed the experiments. P.B.-C.L. performed the ELISA experiments. B.T.C. performed the microglial depletion experiments and provided the samples for analysis for this project. S.S.P. performed the flow cytometry experiments. P.B.F. maintained the animal resources and breeding programs. C.A.L.-R., N.J.-G., and P.M. provided and analyzed the human samples. All the authors assisted in editing the manuscript.

DECLARATION OF INTERESTS

The authors declare no competing interests.

SUPPLEMENTAL INFORMATION

Supplemental information can be found online at https://doi.org/10.1016/j.celrep.2024.114488.

Codocedo et al. find that the gene dosage of microglial HK2 displays differential effects on microglial phenotypes and AD progression. They show that HK2 can regulate inflammation through different non-metabolic activities that are dependent on its subcellular compartmentalization.

Graphical abstract

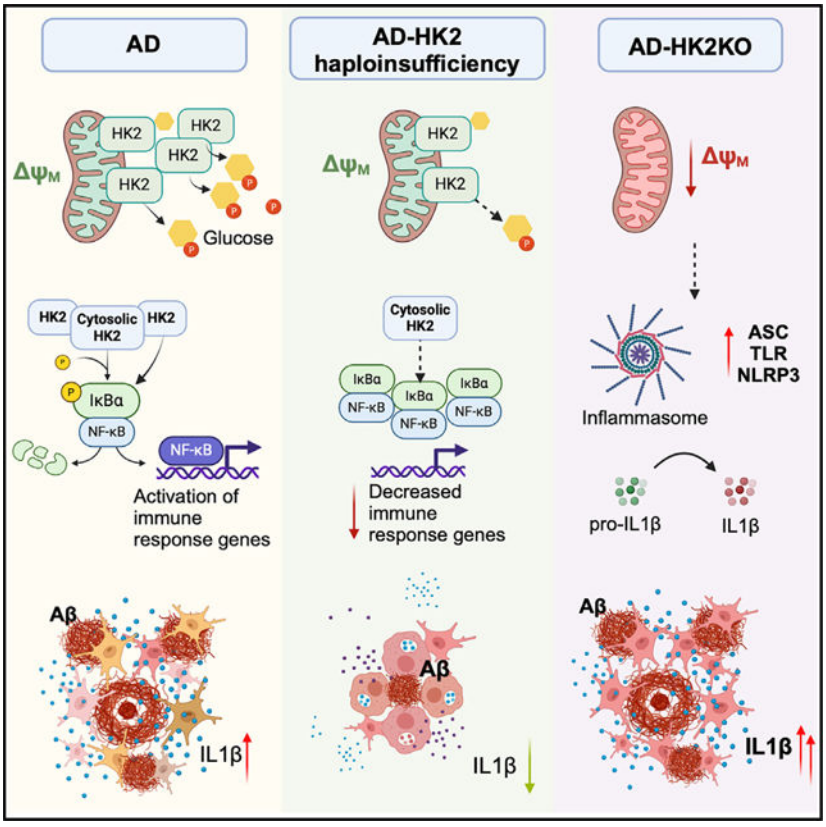

INTRODUCTION

Alzheimer's disease (AD) is a highly prevalent neurodegenerative disorder and the most common cause of dementia in the elderly. AD pathology is characterized by amyloid β (Aβ) deposits and neurofibrillary tangles, both linked to neuronal death and cognitive decline. In the AD brain, a subset of microglia respond to amyloid deposition by migration to the nascent plaque, where they proliferate[1] and subsequently envelop the plaque with their processes, constituting a biological barrier segregating the plaque from the brain parenchyma.[2] The plaque-associated microglia undergo a dramatic morphological transformation that ultimately accompanies the acquisition of a proinflammatory phenotype, releasing neurotoxic factors such as cytokines and an array of immune mediators. More recently, microglial activity has been associated with the seeding and spreading of new Aβ plaques[3] and tau aggregates.[4] The microglial response to AD pathology is highly complex, with the exhibition of phenotypes associated with both disease exacerbation and

mitigation that change with disease progression, which has confounded the understanding of its mechanistic basis and the effects of potential therapies.[5]

It has only recently been appreciated that the plaque-associated microglia undergo a fundamental reprogramming of cellular metabolism necessary to power the manifold phenotypic changes, and cellular activities are integral to their changing bioenergetic and biosynthetic needs.[6–8] Homeostatic microglia employ mitochondrial oxidative phosphorylation to produce cellular ATP. In contrast, microglia respond to immune stimuli by shifting to aerobic glycolysis, which allows the rapid generation of ATP and other metabolic intermediates that subserve the change in microglia phenotypes.[9,10] However, because glycolysis is metabolically inefficient, persistent reliance on glycolysis is postulated to lead to impaired immune function generally associated with chronic and exaggerated inflammatory responses.[11] During the past decade, several studies have described numerous mechanisms by which glycolysis orchestrates inflammation.[12] It has only recently been appreciated that glycolytic enzymes can regulate inflammation by gaining non-metabolic functions that have gone undetected previously.[13] These non-traditional mechanisms can be initiated by changes in the subcellular localization of glycolytic enzymes, allowing them to bind and modify the activity of different inflammatory regulators.[14,15] These non-metabolic activities add a new layer of regulation (complexity) to the relation between metabolism and inflammation.

Hexokinases perform the first and rate-limiting step in glycolysis through the irreversible phosphorylation of glucose to glucose-6-phosphate (G-6-P). The phosphorylated form of glucose is trapped inside the cell and is then metabolized by glycolysis to generate ATP.[16] Hexokinase 2 (HK2) has non-metabolic roles that can impact inflammation independent of its canonical glycolytic role, like other glycolytic enzymes. HK2 binds to the outer mitochondrial membrane (OMM) through direct interaction with the voltage-dependent anion channel (VDAC), and its displacement induces the formation of a mitochondrial pore that triggers the activation of the Nod-, LRR-, and pyrindomain containing 3 (NLRP3) inflammasome.[17]

Recent publications demonstrate the role of HK2 as a critical determinant of microglial metabolism and immune response in various pathological processes.[18–20] However, these independent studies reported conflicting data concerning the effect of genetic inactivation of both alleles of the HK2 gene on microglial phenotypes and disease progression. The discrepancy is also mechanistic, as both groups present diametrically conflicting results in their *in vitro* assessment of ATP levels and use of alternative fuels by HK2-deficient microglia.[18,19] Thus, there is no consensus on the role of microglial HK2 in brain disease, and its role in maladaptive inflammation remains poorly understood.

In this study, we investigated the effects of HK2 gene dosage on regulating microglial phenotypes and AD progression in 5xFAD mice. Its inducible deletion modulates specific features of the microglial response in a gene-dose-dependent manner. In agreement with the report of Hu et al.,[19] the complete loss of HK2 results in a robust inflammatory phenotype that in the 5xFAD mice fails to alter Aβ plaque burden or attenuation of cognitive decline. HK2 haploinsufficiency has very different effects: attenuating inflammation, reducing Aβ

plaque load, and reversing disease-related cognitive decline. Importantly, we found that pharmacological inhibition of HK2 mimics the beneficial effects of HK2 haploinsufficiency and partial loss of function in male 5xFAD mice during the early stages of the disease, suggesting a common mechanism and that its targeting has therapeutic potential.

In our hands, the beneficial effects of the partial antagonism of HK2 were not associated with increased levels of ATP or lipoprotein lipase (LPL) upregulation, as previously proposed.[18] Instead, we observed that the decreased catalytic activity of HK2 was associated with increased levels of its cytosolic target IKBα (also known as "nuclear factor of kappa ligth polypeptide gene enhancer in B-cell inhibitor alpha," or "NFKBIA"). This regulatory protein inhibits the nuclear translocation of NF-κB and the induction of the expression of inflammasome genes. In contrast, the complete deletion of HK2 overrode this mechanism by inducing mitochondrial dysfunction and inflammasome activation, as previously described by Hu et al. and others.[17,19,21]

RESULTS

HK2 expression is selectively induced in Aβ-plaque-associated microglia

We first evaluated the expression of the predominant HK isoforms in the cortex of 5xFAD mice during disease progression. We found that the levels of HK2 were significantly increased in the 5xFAD mice compared to non-transgenic mice at as early as 4 months and at 4-fold higher levels by 8 months of age (Figures 1A–1C). The changes in HK2 were significantly more significant in female 5xFAD mice than in males (Figures 1A–1C), consistent with female 5xFAD mice exhibiting higher levels of Aβ and augmented inflammation.[22] In contrast, the levels of the ubiquitously expressed HK1 were unchanged with disease progression (Figures 1B and 1C).

To confirm that the increase in the levels of HK2 in the cortex is driven exclusively by microglia, we depleted microglia by treatment with the colony-stimulating factor 1 receptor (CSF1R) antagonist PLX5622,[23] which resulted in a complete loss of HK2 induction with no effect on HK1 (Figures S1A and S1B). Furthermore, following inhibitor withdrawal and microglial repopulation, we observed a complete restoration of HK2 levels (Figures S1A and S1B). Flow cytometry analysis showed a significant increase in the cellular expression of HK2 in microglia ($CD11b^+$, $CD45^+$) in 8-month-old 5xFAD mice compared to their non-transgenic controls (Figures S1C and S1D).

To determine the identity of the microglial subpopulation responsible for the HK2 increase, we performed immunohistochemical (IHC) studies of the subiculum and cortex of 8-month-old 5xFAD mice and non-transgenic controls. In the BL/6 mice, staining with IBA1 revealed evenly tiled, ramified microglia, and these homeostatic cells displayed faint somatic staining for HK2 (Figure 1D, top). In contrast, 5xFAD mice at 8 months of age exhibited clustered, plaque-associated microglia with an ameboid morphology generally associated with disease-associated microglia (DAM) or microglial neurodegenerative (MGnD) phenotypes.[24,25] This subset of microglial cells exhibits increased immunofluorescence for HK2 throughout the microglial soma and processes that envelop the plaques (Figures 1D, bottom, and 1E). The regional increase in HK2 levels is directly associated with the amyloid load, with the

subiculum and layer 5 of the cortex exhibiting higher levels of HK2 (Figures S1E and S1F). These observations suggest that the induction of HK2 was triggered by direct contact of the microglia with deposited amyloid and could explain the time-dependent induction of HK2 in the 5xFAD brain.

To determine whether these changes are conserved in human disease, we evaluated HK2 levels in the cortex of AD patients. As expected, we observed a significant increase in HK2 levels in the microglia in close association with Aβ plaques (Figures 1F and 1G). Like our animal studies, qPCR analysis shows that the increase in HK2 levels was significantly more significant in women than in men (Figure 1H).

To confirm our observation through independent databases, we evaluated the expression of HK2 in human AD (hAD) using the Gene Expression Omnibus (GEO) database: GSE33000. We found that the levels of HK2 are increased in the prefrontal cortex of a cohort of 310 human patients. When we segregated the data by sex, the increase in women was significantly higher than in men (Figure 1I). In addition, we observed that the levels of HK1 isoform are diminished, possibly due to neurodegeneration (Figure S1G). Similar findings are reported by the Accelerating Medicines Partnership–Alzheimer's Disease (AMP-AD) consortium, which comprises the currently largest collaborative postmortem brain RNA-sequencing (RNA-seq) project. When the data are segregated by sex, women display an increase in HK2 in the dorsolateral prefrontal cortex and the parahippocampal gyrus (Figure S1H). No brain region was significantly upregulated for HK2 expression in men (Figure S1I; https://agora.ampadportal.org; accessed April 2024).

Remarkably, co-expression network analysis provided by Agora reveals that HK2 is upregulated in the brain of AD patients in concert with several microglial genes (77% of the network, Figure S1J) associated with neurodegeneration, including C1q, C3,[26] spp1,[27] and Toll-like receptor 2 (TLR2),[28] among others (Figure 1J). Gene ontology analysis shows that the primary biological process related to this "HK2/hAD network" involves immune responses and regulation of metabolic processes (Figure 1K), suggesting a crucial role for human HK2 as a hub between metabolism and microglial function. These results suggest that the microglial upregulation of HK2 observed in the 5xFAD mice is conserved in patients with AD and represents a potential therapeutic target. The sex difference observed in HK2 upregulation is consistent with the hypothesis that microglial metabolism plays a central role in the sexual dimorphism of AD[29,30] and highlights the need to include both sexes in the assessment of potential disease-modifying agents.

Gene dosage of microglial HK2 selectively modulates the immune response and disease progression

To directly dissect the role of HK2 in controlling microglial immune response during AD progression, we generated mice with a conditional deletion of one or two copies of the HK2 gene in microglial cells by crossing 5xFAD; CX3CR1-Cre^{ERT2} mice with mice harboring a floxed HK2 allele.[31]

We induced the microglial deletion of one or both HK2 alleles (termed 5xFAD; HK2$^{Fl/WT}$ or 5xFAD; HK2$^{Fl/Fl}$, respectively) by intraperitoneal (i.p.) injection of tamoxifen (TAM) at 2

months of age (Figure 2A), a period at which amyloid deposition and microgliosis begin.[32] Mice harboring the Cx3cr1-Cre^{ERT2} cassette but lacking the *LoxP* sites in HK2 were treated with TAM and used as controls (5xFAD; HK2$^{WT/WT}$). Three months later (5 months of age), we evaluated AD pathogenesis (Figure 2A).

By bulk qPCR analysis, we observed that TAM treatment induced the specific recombination of HK2 with no changes in the ubiquitous HK1 gene (Figures 2B and 2C). However, our bulk analysis showed no difference in HK2 mRNA level between hemizygote and homozygote HK2 knockouts (KOs) (Figure 2B). Because the Cx3cr1Cre^{ERT2} line has an effectiveness of 89% and bulk analysis is not able to detect individual recombination events,[33] we used IHC analysis in tissue to evaluate, at the protein level, the level of HK2 recombination. Figures 2D and 2E show that the protein levels of HK2 are significantly reduced in the HK2$^{Fl/Fl}$ microglia compared to the levels observed in the HK2-haploinsufficient and wild-type (WT) mice.

We evaluated the effect of microglial HK2 gene dosage on the cortical levels of Aβ. ThioS staining revealed that microglia haploinsufficient in HK2 elicited a robust reduction in the dense core plaque burden compared to HK2-sufficient littermates (Figures 2D and 2F). Similarly, we observed a significant decrease in the microglial coverage area (Iba1^{+} cells) as a proxy for microglial density (Figures 2D and 2G). Remarkably, the complete deletion of HK2 resulted in an phenotype opposite that observed in mice haploinsufficient for HK2, as the HK2-null mice were characterized by an increased number of plaques and plaque-associated microglia (Figures 2D–2F and 2G). Consistently, western blot analysis of soluble fractions of the cortex of our transgenic mice mirrored the diverging effects of HK2 copy number in the levels of Aβ species detected with the MOAB2 antibody, as well as the microglial marker triggering receptor expressed on myeloid cells 2 (Trem2) (Figures 2H–2O). Trem2 is an essential factor for microglial activation and barrier formation.

Nevertheless, recent studies have reported that suppressing TREM2 expression with antisense oligonucleotides significantly reduced plaque deposition when evaluated 1 month after injection in APP/PS1 mice.[34] Furthermore, Meilandt et al. reported that Trem2 haploinsufficiency in the PS2APP AD mouse model displays sufficient microglial Aβ coverage to enable plaque compaction and neuroprotection.[35] This suggests that the attenuation of microglial activation induced by HK2 haploinsufficiency is consistent with improvement in AD pathology early in the adult stage.

To evaluate if the alteration in the expression of HK2 affects cognition, we evaluated the working memory of the 5xFAD mice as assessed by their spontaneous alternation in a Y maze.[36] The partial loss of HK2 significantly improved the cognitive performance of the mice (Figure 2P). Once again, the loss of both HK2 alleles had little effect on cognition, as the spontaneous alternation rate was like that of the control 5xFAD; HK2$^{WT/WT}$ mice (Figure 2P). No noticeable sex differences were observed upon genetic inactivation of the HK2 gene.

To ascertain the cellular and molecular pathways affected by HK2 deficiency during AD progression, we performed a transcriptional analysis of the cortical samples with NanoString

at 5 months of age. We used a glia panel that evaluates the expression of 770 genes, allowing us to perform gene set enrichment analysis (GSEA) to quantify cell populations defined by their corresponding marker gene set in each sample. The reduction in gene dosage of HK2 resulted in dramatically different outcomes, with HK2 haploinsufficiency shifting the expression of microglial genes toward homeostatic phenotypes (Figure 3A). Conversely, the loss of both HK2 alleles did not affect the transcriptional landscape of the 5xFAD microglia. With a less conservative analysis ($p < 0.05$ instead of adj-$p < 0.05$), we observed changes in only three genes that pointed to a detrimental effect, as the mitochondrial arginase type 2 (Arg2) was decreased. α-synuclein and KLK6, a protease that participates in the cleavage of APP, were upregulated (Figure 3B).

The effect of HK2 haploinsufficiency impacted the enrichment of gene sets associated with microglial activation and the transition to neurodegenerative states. GSEA of 5xFAD; $HK2^{Fl/WT}$ mice showed a reduction in the MGnD/DAM signature genes as well as the complement system genes (Figure 3C). Importantly, cell-type profiling revealed that the only cell type affected by HK2 partial loss of function was microglia, confirming the cellular specificity of HK2 actions in our mouse model and reinforcing the notion that the antagonism of HK2 attenuates the microglial response during AD progression without notable effects in other cells in the brain (Figure 3D). This reduction in the enrichment of microglia is consistent with the reduced microglial abundance as demonstrated by IHC analysis (Figure 2G).

To directly evaluate the transcriptional effect of HK2 dosage on the microglial gene expression, we performed incubations of primary cultures of microglia derived from our transgenic mice with the active metabolite of TAM (4-hydroxytamoxifen [4-OHT]) (Figure 3E). In this *in vitro* experimental setting, we corroborated that a set of genes associated with immune activation and inflammation (including LPL, interleukin-1β [IL-1β], Trem2, TLR2, and genes of the complement system) exhibited reduced expression in the HK2-haploinsufficient microglia (Figure 3F). Remarkably, the same set of genes displayed an increase, with respect to controls, in the double-KO HK2 microglial cells (Figure 3F).

Our results suggest that the HK2 expression level governs microglial phenotype, regulating critical disease-related responses, such as microglial gene expression, affecting deposited and monomeric amyloid.

The pharmacologic inhibitor of HK2, lonidamine, modulates the microglial response and amyloid pathology in a sex-dependent manner in the 5xFAD mice

To assess the therapeutic potential of HK2 inhibitors, we evaluated the acute effect of its pharmacological inhibition in the 5xFAD mice. Several drugs have been developed as HK2-specific inhibitors.[37] The best characterized is lonidamine (LND), an orally administered small molecule that inhibits glycolysis by the preferential inactivation of HK2.[38] LND has been used in several clinical trials in cancer in the United States and is currently approved in Europe for this indication.[37] LND is a selective blocker of glycolysis in tumor cells with minimal effects on normal cells and an acceptable side-effect profile.[39]

We treated 5xFAD mice at different stages of disease for 7 consecutive days with a daily i.p. injection of 50 mg/kg LND. Control mice (BL/6 and 5xFAD littermates) were injected with the vehicle. The treatment did not affect the body weight of the mice during the treatment period (Figure S2A).

In males at 5 months of age, LND treatment induced a significant reduction in the cortical levels of (fibrillar Aβ) fAβ, as revealed by ThioS staining (Figures 4A and 4B). Similarly, we observed a significant reduction of the cortical microglial area ($IBA1^+$ cells), reflecting a decrease in microgliosis (Figure 4C). However, the remaining plaques observed in the cortex retained abundant plaque-associated microglia and sustained barrier integrity, as the microglial coverage of Aβ plaques was not different between groups (Figure 4D). The preservation of the barrier integrity was functionally validated by evaluation of the area occupied by swollen $Lamp1^+$ dystrophic neurites, which was reduced in the male LND group, suggesting an improvement in neuronal integrity, despite the overall decreased microgliosis (Figures 4A and 4E).

Western blot analysis of the soluble fraction of the cortical lysate corroborated the effect of HK2 inhibition on amyloidosis, as fibrillar Aβ42 was dramatically reduced in the male 5-month-old 5xFAD mice treated with the HK2 inhibitor (Figures 4F and 4G) and almost undetectable at 3 months (Figures S2B and S2C). We also observed a significant reduction in the levels of Trem2, suggesting attenuation of microglial activation (Figures 4F and 4G). However, the 7-day treatment failed to reduce the cortical amyloid burden or Trem2 levels at 8 months (Figures S2F–S2I), which is consistent with the idea that microglial intervention is more effective during the early stages of the disease.[40,41]

These findings are similar to those recently reported by Leng et al. However, that study only included 5xFAD males evaluated at 6 months.[18]

Unexpectedly, the same treatment failed to reduce the female cortex's amyloid, microgliosis, and neuronal dystrophy (Figures 4J–4N). Western blot analysis of the cortical lysates with the anti-Aβ antibody MOAB2 showed no changes in amyloid burden with the drug treatment. Still, it resulted in a significant increase in the levels of HK2 and Trem2, suggesting an increase in the activation state of microglia. This trend was also observed at 3 months (Figures S2B–S2E), suggesting that the observed differences between sexes were not attributable to an excessive amyloid burden in females, as at 3 months, the cortical amyloid load is lower than that observed in the 5-month-old male cortex.[42] Analogous to that observed in males, the acute treatment with LND failed to induce changes in amyloid levels in the female cortex at 8 months (Figures S2F–S2I).

To ascertain the cellular and molecular pathways affected by HK2 inhibition, we performed a transcriptional analysis of the cortical samples with NanoString. Our bulk RNA analysis confirmed the sex-biased phenotype of microglia induced by LND, as females exhibited increased levels of several microglial genes associated with induction of an immune response, including Trem2, Tyrobp, Spp1, CD68, and complement-related genes, compared to males at 5 months of age (Figure 5A). Complementary qPCR analysis corroborated these opposite changes for selected DAM markers (Figure 5B). GSEA showed that the significant

differences in the biological processes between sexes are related to their activation status, with females showing a higher expression of MGnD/DAM signature genes as well as the one associated with primed microglia and the complement system (Figure 5C). This observation suggests that LND treatment induces sex-specific effects in the microglial activation of 5xFAD mice. This was further supported by cell-type profiling, which, like our IHC analysis mentioned above (Figures 4C and 4L), showed a reduced microglial abundance in males compared to females with no detectable changes in other cell types. These data also confirm the cellular specificity of HK2 and its targeting with LND (Figure 5D).

The altered number of microglia between sexes could affect this bulk gene expression analysis. To further evaluate the direct effect of LND on microglial gene expression, energy production, and viability, we performed incubations with LND in primary cultures of microglia for 24 h (Figure 5E). In this experimental setting, in which each culture is derived from individual mouse pups, the sex effect was completely lost, as we observed a significant and consistent reduction in the mRNA expression of inflammatory cytokines (IL-1β, IL-6, and tumor necrosis factor [TNF]), complement proteins, and the DAM markers spp1 and APOE (Figure 5F). In addition, the expression of HK1 as well as homeostatic markers like transforming growth factor B1 (TGFB1) and TGFBR1 were not affected (Figure 5F), which is a profile comparable to that observed only in males treated *in vivo.*

Different factors have been proposed to explain the clinical sex differences observed in the incidence of AD, response to treatments, and occurrence of side effects.[43] Among these factors, sex differences in drug pharmacokinetics and brain exposure have been proposed to explain the 2-fold incidence of adverse drug reactions in women compared to men.[44] We compared the LND brain levels in both sexes to determine potential differences in biodistribution that could explain the opposite microglial phenotypes observed *in vivo*. High-performance liquid chromatography-tandem mass spectrometry (HPLC-MS/MS) analysis found that in females, the brain concentrations of LND were double (94.29 ± 16.15 ng/g) that in males (45 ± 10.47 ng/g), despite comparable blood concentrations (Figure 5G).

We do not know if this differential brain concentration is due to differences in blood-brain barrier (BBB) integrity, transport, or brain metabolism of LND. However, this finding suggests that the sex-biased effect of LND on microglial phenotype may depend on its concentration levels in the brain. We speculate that lower levels of HK2 inhibition induce an attenuation of microglial activation, like the one observed with our HK2 heterozygous mice. Conversely, a higher concentration of LND in the brain could exacerbate microglial activation by the complete inactivation of HK2, as observed with our HK2Fl/Fl mice, or by off-target drug effects. These results could also explain the lack of divergent effects observed *in vitro* tested at a single dose of LND (200 μM). However, we cannot discount the impact of additional factors (i.e., hormones) in the induction of opposite phenotypes *in vivo*, as these were also absent in our *in vitro* studies.

Further experiments are necessary to determine the basis of differential LND distribution in the brain and if an analogous situation is observed in humans. Finally, we note that LND has also been reported to inhibit additional targets, like the mitochondrial monocarboxylate transporter 4 (MCT4).[45,46] Remarkably, co-expression network analysis of RNA-seq data

from the AMP-AD consortium (Agora platform) showed that MCT4 (also known as SLC16A3) is co-expressed with HK2 and several other microglial genes associated with neurodegeneration in the brain of AD patients (highlighted in yellow in Figure 1J). MCT4 is predominantly expressed by microglia and involved in mitochondrial function; thus, LND targets the same biological process in the same cellular population. Sex differences in the expression or function of MCT4, as well as other uncharacterized targets, can also be involved in the sex-biased response of microglia to LND treatment.

A protective phenotype of microglia induced by HK2 antagonism is not associated with increased ATP content or mitochondrial binding of HK2

Multiple mechanisms have been proposed to explain the role of HK2 in modulating the inflammatory responses of microglia/macrophages, including its metabolic actions and newly recognized alternative mechanisms arising from its regulated association with mitochondria.

It has recently been argued that microglial HK2 antagonism dramatically boosted ATP production exclusively within microglia through a compensatory shift to LPL-dependent lipid metabolism, increasing Aβ phagocytosis in murine AD models.[18] However, a second independent study by Hu et al.[19] arrived at quite different conclusions. They found that microglial HK2 depletion reduced levels of cellular ATP and boosted mitochondrial dysfunction,[19] a setting that would not support increased mitochondrial β-oxidation of lipids.

Because our phenotypic characterization showed that the beneficial effects in the 5xFAD mouse were observed upon partial antagonism of HK2, we evaluated ATP content in microglia haploinsufficient for HK2 or microglia treated with the inhibitor LND. In both conditions, the HK activity was significantly reduced (Figures 6A and 6B). However, the *in vitro* measurements of ATP levels show disparate results, with no changes in ATP content observed in primary cultures haploinsufficient for HK2 (Figure 6A). In LND-treated cells, we observed a dose-response decrease in the levels of ATP that was significant at 200 μM LND (Figures 6B and S4A). Cellular metabolism was evaluated by 3-(4,5-dimethylthiazol-2-yl)-5-(3-carboxymethoxyphenyl)-2-(4-sulfophenyl)-2H-tetrazolium (MTS) assay, which measures the activity of mitochondrial NAD(P)H-dependent dehydrogenase enzymes in metabolically active cells.[47] No changes were observed with HK2 partial loss or between 50 and 200 μM LND (Figures 6A, 6B, and S4B), suggesting that cells were viable and mitochondrial function was unaffected in these conditions. Higher LND concentrations (>500 μM) elicited cellular toxicity, which also reflects a massive drop in ATP levels (Figure 6B). We conclude that the beneficial effects of HK2 partial antagonism are not dependent on elevated ATP production.

We further explored the effect of HK2 antagonism on microglial mitochondria by evaluating their membrane potential, which reflects the process of electron transport and oxidative phosphorylation, the driving force behind ATP production. In primary cultures of microglia derived from $HK2^{Fl/Fl}$ mice, staining with MitoTracker Deep Red (DR) revealed a significant decrease in their mitochondrial potential after HK2 deletion (Figures 6C and

6E). However, LND treatment of primary microglia did not affect this parameter (Figures 6C and 6D).

In vivo, we evaluated the microglial mitochondrial potential by flow cytometry of $CD11b^+$ and $CD45^+$ cells derived from the brains of our 5xFAD mice. In 5-month-old mice, neither HK2 haploinsufficiency nor LND treatment had significant effects on the number of activated microglia positive for MitoTracker DR (histograms) or in its fluorescence intensity (Figures 6F and 6G), implying that the partial antagonism of HK2 attenuates its catalytic activity without the mitochondrial side effects observed with its total deletion. These results suggest that the differential effect of HK2 gene dosage on mitochondrial dysfunction, an essential trigger of the inflammasome activation, could explain the opposite microglial response observed in AD because of HK2 copy number.

Finally, we studied the *in vivo* co-localization of HK2 and VDAC in the 5xFAD mice. In 5-month-old mice, we observed a significant decrease in HK2 mitochondrial association in plaque-associated microglia compared to unaffected parenchymal microglia (Figures 6H and 6I). As this phenomenon has been proposed as an essential inflammatory trigger, we expected that LND treatment might revert the amyloid-induced cytosolic translocation of HK2. However, LND failed to revert this pathological effect (Figures 6H and 6I), arguing that the mechanisms by which HK2 partial antagonism regulates inflammation and disease progression are independent of its mitochondrial association and could be due to the inhibition of HK2 cytosolic actions.

HK2 partial antagonism reduces the expression of inflammasome elements and the Aβ-induced nuclear translocation of NF-κB

Microglia are multifaceted cells that participate in AD pathogenesis through many distinct mechanisms, including phagocytosis and clearance of Aβ, as well as the induction of neuroinflammation and the spreading of Aβ.[48] Primary cultures of murine microglia and human microglia clone 3 (HMC3) cells treated with LND increased their uptake of Aβ, as revealed by western blot and MOAB2 staining (Figures S3A, S3B, S4C, and S4D) as previously reported. However, flow cytometry of microglia revealed that LND did not affect the percentage of phagocytic cells or levels of internalized Aβ, as evaluated by methoxy-X04 uptake (Figure S3C). In addition, we observed that our manipulations of HK2 failed to alter the amyloid burden in brain areas experiencing early accumulation, like the subiculum (Figures S3D–S3G), or when the treatment is done in the symptomatic stage of the disease (8 months of age, Figures S2F–S2I). This suggests that the phagocytic capacity induced by HK2 partial inhibition is necessary but insufficient to eliminate the preexisting amyloid plaques.

It has been proposed that inflammation can impact amyloid formation by seeding activities of some elements of the inflammasome, like the apoptosis-associated speck-like protein containing CARD (ASC) protein.[49] In addition, the production of proinflammatory factors that act to remodel synapses by altering their shape, composition, and density ultimately contributes to the cognitive dysfunction of AD patients[50] (Figure 7A).

Accordingly, we evaluated the expression of the components of the inflammasome pathway described in Figure 7A. qPCR analysis has shown that at 5 months, most inflammasome elements are upregulated in the cortex of the 5xFAD mice (Figures 7B and S3H). According to our previous observations, the treatment with LND induced a sex-biased effect. In males, HK2 inhibition blocked the increase of TLR2, ASC, and the inflammatory effector IL-1β (Figures 7B and 7C). Female mice displayed a polar opposite phenotype, with increased expression of inflammasome components in response to HK2 pharmacological inhibition (Figures S3H and S3I).

As reported above, our genetic approach lost the sex differences in gene expression, but we still observed an HK2 gene dosage effect. 5xFAD mice haploinsufficient for HK2 showed a reduction in the expression of inflammasome elements. In contrast, the double KO displayed an increase in the levels of TLR2 and ASC (Figure 7D). ELISA confirmed the divergent effect induced by HK2 gene dosage on the protein levels of IL-1β (Figure 7E).

Recent reports have suggested that HKs can induce inflammation by a gain of non-metabolic functions associated with inflammasome induction through the NF-κB pathway.[20,44] NF-κB is a master regulator of innate and adaptive immune functions that plays a critical role in the expression of various proinflammatory genes, including inflammasome regulation[52] (Figure 7A). Moreover, NF-κB has been described as a downstream target of metabolic sensors, and its transcriptional activity can be regulated by inhibitors of glycolysis in microglia challenged with lipopolysaccharide (LPS).[12] We explored an HK2 non-metabolic mechanism recently described in cancerous cells.[51,53] This mechanism involves a cytosolic gain of function for HK2 in which the binding and phosphorylation of IKBα, a cytosolic repressor of NF-κB, results in IKBα degradation and subsequent nuclear translocation of NF-κB (Figure 7F). To test if this mechanism was conserved in microglia, we evaluated the expression of IKBα in cortical samples of 5xFAD mice haploinsufficient for HK2. At 5 months, there were no changes in the mRNA levels of IKBα (Figure 7I). Still, its protein levels were significantly upregulated in the HK2-heterozygous mice (Figures 7G and 7H), suggesting a posttranslational mechanism consistent with the newly described non-metabolic function of HK2 in cancer.[51,53] Next, we treated primary microglia cultures with aggregated Aβ and LND for 24 h to determine the levels of IKBα and nuclear translocation of NF-κB. qPCR analysis revealed again that HK2 inhibition had no effect on IKBα transcription (Figure 7L); however, western blot analysis showed that LND treatment significantly increased its protein levels, even in the presence of Aβ (Figures 7J and 7K). As expected, Aβ treatment induced increased levels of NF-κB in the nuclei of challenged cells compared to vehicle controls; however, the co-incubation with LND prevented this translocation (Figures 7M and 7O), concomitant with increased uptake of Aβ (Figures 7M and 7N). Similar results were observed in HMC3 cells (Figures S4E and S4F). This suggests that HK2's role in stabilizing IKBα and NF-κB signaling is conserved in microglia. These findings substantially expand our understanding of the crosstalk between metabolism and inflammation in the context of neurodegenerative diseases, particularly AD.

Together, these results point to inflammation as a possible mechanism by which HK2 dosage results in opposing functional phenotypes of microglia, influencing AD progression. We argue that the partial antagonism of HK2 regulates microglial responses by affecting the

induction of inflammation by decreasing the NF-κB-mediated expression of elements of the inflammasome and IL-1β; this process seems to be dependent on its catalytic activity and not dependent on the energetic status of the cell. Remarkably, the partial antagonism of HK2 does not affect the mitochondria, suggesting that the mitochondrial-dependent inflammatory pathway was not affected. This is not the case for the complete deletion of HK2, in which the induced mitochondrial deficits are inconsistent with increased ATP production and explain a hyperinflammatory phenotype that exacerbates AD progression.

DISCUSSION

Central to understanding the biological underpinning of the microglial actions in the AD brain is recognizing the importance of disease-induced reprogramming of cellular metabolism. Immunometabolism governs the ability of microglia to mount an immune response and the nature of their effector functions.[6,8,54] Microglia respond to an immune challenge (in this case, exposure to deposited amyloid) by switching from oxidative metabolism to glycolysis to support the acquisition of disease-induced phenotypic states typified by the generation of complex and sustained immune responses.[10,55]

In this study, we tested the hypothesis that targeting key enzymes within metabolic pathways employed by immune-stimulated microglia might provide new therapeutic options for AD. We focused our attention on HK2 because it is a member of a family of enzymes that perform the first and rate-limiting step in glycolysis through the irreversible phosphorylation of glucose, which can be further metabolized by glycolysis to rapidly generate ATP as well as other metabolic intermediates necessary for various biosynthetic pathways.[16] Recent evidence has demonstrated that HKs can regulate inflammation through metabolic and non-metabolic activities.[13]

During the preparation of this article, two independent groups performed analogous studies. Still, they reported conflicting data concerning the effects of HK2 complete deletion and inhibition on microglial ATP levels and microglial responses in murine models of stroke and AD, respectively.[18,19] This discrepancy is relevant, as Leng et al.[18] proposed that the increased ATP levels, through a compensatory shift to lipid metabolism, are instrumental in AD improvement after microglial HK2 inhibition. This proposal, however, conflicts with previous studies done in microglia treated with HK2 inhibitors that describe decreased levels of ATP. Cheng et al. found that 2-deoxy-D-glucose (2-DG) and 3-BP induce an increase in the ADP/ATP ratio of BV2 microglia, which was associated with decreased inflammation.[20] Vilalta and Brown also observed that 2-DG treatment resulted in a rapid depletion of ATP that preceded microglial apoptosis.[56] Hu et al.[19] demonstrated that treatment with 2-DG or 3-BP or the induced deletion of microglial HK2 resulted in a dramatic reduction of ATP, leading to an “energy-deficient state in microglia, with no compensation to glutamine or fatty acid oxidation.”

Our results align better with those reported by Hu and others, as we never observed an increase in the cellular levels of ATP after the antagonism of microglial HK2. Another substantial difference reported *in vivo* was the inflammatory consequence of HK2 complete deletion in neurodegenerative contexts. Leng et al.[18] reported decreased inflammation and

disease improvement in the 5xFAD mice model; meanwhile, Hu et al.[19] demonstrated that HK2 complete deletion exacerbated ischemic damage in a murine stroke model, mainly due to a hyperinflammatory microglial response. Once again, our results align better with those of Hu et al.,[19] as we observed that the double KO of HK2 failed to improve cognition and reduce amyloid in the 5xFAD mice. This was associated with a microglial phenotype characterized by elevated elements of the inflammasome, the complement, and IL-1β production.

Hu et al. proposed that the complete deletion of HK2 in microglia-induced mitochondrial dysfunction as one of its non-metabolic actions is the occlusion of the mitochondrial pore by its binding with VDAC.[19] Similar consequences were also reported in HK2-depleted epithelial cells, which exhibited dramatically reduced mitochondrial respiration, indicating impairments of the mitochondrial electron transport chain.[57] We confirmed that the double KO of HK2 resulted in a significant reduction in the mitochondrial potential, which is directly linked to a reduced capacity of mitochondria to produce ATP. These joined observations are inconsistent with the mechanism proposed by Leng and colleagues,[18] as mitochondrial health is fundamental for the ATP production associated with β-oxidation of lipids. In addition, in macrophages, the lack of HK2 mitochondrial binding is a solid inflammatory trigger, as it allows the release of mitochondrial content that activates the inflammasome and stimulates the production of inflammatory cytokines.[21] This is consistent with the observed expression of inflammasome elements and the increased production of IL-1β observed in our HK2 double-KO mice.

We expanded these studies by characterizing the HK2 heterozygous mice in the 5xFAD context, as we reasoned that a single copy of HK2 can regulate its inflammatory activities without compromising its mitochondrial role. Indeed, the partial loss of HK2 induced an opposite microglial phenotype characterized by reduced inflammation and amyloid burden and improved spatial memory. Notably, neither the partial loss of HK2 nor LND treatment resulted in mitochondrial alterations, suggesting that these manipulations of HK2 specifically target its catalytic activity without significant effects on its non-metabolic function related to mitochondrial integrity. This separation of roles is impossible in the microglia experiencing the complete loss of HK2, as its mitochondrial function depends on its molecular association with the mitochondrial pore in the outer membrane.

In our hands, HK2 partial antagonism did not increase ATP content nor restore homeostatic association with VDAC in the 5xFAD mice. We explored a third mechanism recently described in cancerous cells.[51,53] This mechanism involves a cytosolic gain of function for HK2 in which the binding and phosphorylation of IKBα, a cytosolic repressor of NF-κB, results in IKBα degradation and subsequent nuclear translocation of NF-κB. Consistently, HK2 partial antagonism resulted in elevated protein levels of IKBα that blocked the nuclear translocation of NF-κB. This suggests that this non-metabolic role of HK2 is conserved in microglia, highlighting its multifaceted role in regulating inflammation, particularly during AD progression.

Logically, the final phenotypic output of microglia will be determined by the balance between these different mechanisms regulated by HK2. The complete loss of HK2

represents an extreme state in which mitochondrial dysfunction drives the microglia toward an inflammatory state. Importantly, its partial deficiency has a very different effect, favoring homeostatic states due to reduced NF-κB signaling. This phenomenon has precedent, as Gan and colleagues reported similar observations induced by Trem2 gene dosage on microglial injury response and tauopathy.[58] Moreover, PLCG2, another important AD risk gene, can regulate divergent microglial functions via Trem2 or TLR association,[59] reinforcing the idea that many molecular players can drive microglial phenotypes depending not only on its enzymatic activity but also on its cellular localization and interacting partners.

Overall, our results explain the discrepancies in the literature concerning the outcome of HK2 antagonism in microglial responses and disease progression. By comparing HK2 gene dosage and HK2 pharmacological inhibition, we reveal that, in microglia, HK2 regulates inflammation through metabolic and non-metabolic activities critically dependent on its subcellular compartmentalization. This mechanism allows HK2 to fine-tune the inflammatory response of microglia, strongly suggesting that its targeting is a promising alternative to treat neuroinflammation, particularly AD. Our study also warns about the need to understand the molecular context of HK2 and how variables like age and gender affect these contexts to anticipate the possible phenotypic outcome of its targeting and side effects.

Limitations of the study

While we identify that the partial antagonism of HK2 regulates IKBα levels in microglia, an alternative metabolic mechanism has been described for the regulation of NF-κB signaling and inflammasome activation. For instance, it has been proposed that glucose metabolism regulates proinflammatory NF-κB transcriptional activity through effects on the cytosolic NADH:NAD^+ ratio and the NAD(H)-sensitive transcriptional co-repressor CtBP.[12] Considering the multitude of metabolic and non-metabolic roles of HK2, determining the exact contribution of the different molecular mechanisms that drive the observed *in vivo* phenotypes needs further exploration.

The use of Cx3cr1CreERT2 is justified by its high efficiency over other Cre lines; however, one limitation of its use is associated with induced recombination of $LYVE^+$ brain border macrophages,[33] which potentially can have some participation in the observed phenotypes.

STAR★METHODS

RESOURCE AVAILABILITY

Lead contact—Further information and requests for resources and reagents should be directed to and will be fulfilled by the lead contact, Gary E. Landreth (glandret@iu.edu)

Materials availability—This study did not generate new unique reagents.

Data and code availability

- This paper utilizes existing, publicly available data. Accession numbers for the datasets are listed in the key resource table. Flow cytometry, microscopy, and western blot data are available upon request.

- This paper does not report original code.
- Any additional information required to analyze the data reported in this paper is available from the lead contact upon request.

EXPERIMENTAL MODEL AND STUDY PARTICIPANT DETAILS

Mice—Mice were housed at the Indiana University School of Medicine (IUSM) animal care facility and were maintained according to USDA standards (12-hr light/dark cycle and food and water *ad libitum*), per the Guide for the Care and Use of Laboratory Animals (National Institutes of Health, Bethesda, MD).

We used 5xFAD mice which express five human familial Alzheimer's disease mutations driven by the mouse Thy1 promoter (Oakley et al., 2006) (The Jackson Laboratory [B6SJL-Tg (APPSwFlLon, PSEN1*M146L*L286V) 6799Vas, Stock #34840-JAX]). 5xFAD mice as well as its healthy littermate control (C57BL/6J wild-type mice) were aged to 4, 6 and 8 months to model disease progression.

To generate an AD mice model that conditionally inactivate HK2 expression in microglia, we crossed 5xFAD mice expressing cre only in myeloid cells over the CX3CR1 promoter (5xFAD:CX3CR1-creERT2) with mice bearing one or two floxed alleles of HK2 (HK2flox/flox) (Patra et al., 2013).

The resulting 5xFAD: CX3CR1-creERT2:HK2flox/wt and 5xFAD: CX3CR1-creERT2:HK2flox/Flox mice (termed 5xFAD:HK2Flox/wt and 5xFAD:HK2Flox/wt respectively) were treated with tamoxifen at 2 months to induce recombination and then aged to 5 months to assess the effect of HK2 haploinsufficiency in disease presentation. 5xFAD: CX3CR1-creERT2:HK2wt/wt mice were equally treated with TAM and used as control. All mice were maintained on a C57BL/6 J background. In this study, both male and female mice were used for all experiments.

Human samples—Post-mortem brain tissues from control and AD patients were provided in the form of frozen blocks by the Brain Resource Center at Johns Hopkins. AD cases consisted of pathologically severe AD, stage V–VI.

Cell lines and primary cultures—Protocol of primary neonatal microglia cultures was adapted from (Saura et al., 2003). Briefly, brains from 1 to 3-day-old C57BL/6J mouse pups were isolated and processed individually. The individual brains were then dissociated by mechanical disruption using a nylon mesh and cells were plated in a six-well-plate in advanced DMEM-F12 medium containing 10% FBS, 1% glutamax and 1% penicillin-streptomycin. Every seven days, medium was replenished. After 3 weeks, mixed glial cultures reached confluence and were isolated by mild trypsinization. Briefly, cells were washed with culture medium without FBS and treated with a mixture of trypsin (0.25% without EDTA) and DMEM-F12 medium in a 1:3 ratio. After 15 min incubation, astrocytic cell layer detached and left a layer of microglia attached to the bottom of the culture dish. Microglial cells were maintained in mixed glial cell media for 2 to 3 extra days.

METHOD DETAILS

Drug treatments—PLX5622 was provided by Plexxikon formulated in AIN-7 diet at 1200 mg/kg. At 4 months of age, either normal rodent diet or PLX5622-containing chow was administered for 28 days. An additional cohort of 4-month-old mice were treated with PLX5622 or control diet for 28 days, then discontinued from PLX5622 feed and treated with a normal rodent diet for an additional 28 days. At 6 months of age, this cohort of mice was euthanized, and molecular analyses were performed. Experiments always used littermate controls.

Lonidamine was purchased from Cayman Chemicals (14640) and stock solution was prepared in DMSO (Sigma D2650). The daily dose of LND used was 50 mg/kg body weight diluted in PBS1x (DMSO 0.05%) and was injected intraperitoneally into 5-month-old 5xFAD mice in 1 ml volume, for 7 consecutive days. The drug as well as the vehicle solution was well tolerated and did not affect the body weight of the mice. For *in vitro* experiments, 200 μM of LND was added to the media 30 min prior to its co-incubation with FAβ (5 μM). For gene expression analysis, the primary cultures were incubated with the same concentration of LND for 24 hrs. For hexokinase activity, cellular lysates were incubated for 1h with LND or vehicle with was measured using a hexokinase assay kit (Abcam, ab211103) according to manufacturer instructions.

Tamoxifen was obtained from Sigma (T5648). Stock solutions were prepared in vehicle (10% Ethanol (Sigma E7023) + 90% corn oil (Sigma C8267)) and stored protected from light at −20 °C. The daily dose of TAM used was 15 mg/kg body weight and was injected intraperitoneally into 2-month-old 5xFAD mice in 0.1 ml volume, for 5 consecutive days.

Spontaneous alternation Y-maze test—Mice were acclimated to the testing room under ambient lighting conditions for 1 h. Spontaneous alternation performance was tested using a symmetrical Y-maze. Mice were placed in the center of the Y-maze and the sequence of entries into each arm was recorded via a ceiling-mounted HD camera integrated with behavioral tracking software (ANY-maze. Stoelting, CO, USA). Each mouse was placed and was allowed to explore freely through the maze during an 8-min session. The sequence and total number of arms entered were recorded. Arm entry was complete when the hind paws of the mouse had been completely placed in the arm. Percentage alternation was calculated as the number of triads containing entries into all three arms divided by the maximum possible alternations (the total number of arms entered minus 2) × 100. After behavioral testing, mice were sacrificed for biochemical and histological analysis.

Collection of tissue and tissue homogenization—Following treatment, animals were anesthetized and euthanized according to the IUSM Institutional Animal Care and Use Committee-approved procedures. After transcardial perfusion with PBS 1X, mouse brains hemispheres were divided for immunohistochemistry (IHC) studies and homogenization. One hemisphere was fixed by overnight with 4% PFA at 4 °C. Then, brains were cryoprotected in 30% sucrose at 4 °C and embedded. Brains were processed on a cryostat as 30 μm free-floating sections. The other hemisphere was homogenized in Tissue homogenization buffer (THB) supplemented with protease inhibitor cocktail. One portion of

the homogenate was further sonicated for protein extraction and western blot and ELISA analysis, and the other was stored at −80 °C in RNA bee (Amsbio, CS-501B) for RNA extraction and gene expression analysis.

Post-mortem brain tissues from patients with AD were homogenized in RIPA buffer with a protease inhibitor cocktail (Roche) and a dilution of brain to RIPA of 1:10 (w/v). Samples were then centrifuged at 13,200 rpm for 15 min at 4°C. The supernatants were portioned into aliquots, snap-frozen, and stored at −80°C until analyzed. The RIPA-insoluble pellet was treated with formic acid by mixing samples with 88% formic acid for 1 hr at room temperature (the volume of 88% FA was one-fourth of the volume used for RIPA). Samples were then diluted with distilled water to obtain the same volume used in RIPA and lyophilized for 24 hr. Freeze-dried samples were reconstituted in PBS using the same volume that was originally used for RIPA. Samples were then sonicated for 30 s. Finally, samples were mixed with running buffer, run on a gel, and analyzed by western blot.

Immunostaining, image acquisition, and image analysis—For immunostaining, at least three matched brain sections were used. Free-floating sections were washed and permeabilized in 0.1% Triton in PBS (PBST), followed by antigen retrieval using 1x Reveal decloacker (Biocare medical) at 85 °C for 15 min. Sections were blocked in 5% normal donkey serum in PBST for 1 h at room temperature (RT). Primary antibodies were incubated in 5% normal donkey serum in PBST overnight at 4 °C. Sections were washed and visualized using respective species-specific AlexaFluor fluorescent antibodies (diluted 1:1000 in 5% normal donkey serum in PBST for 1 h at RT). Sections were counterstained and mounted onto slides. For thioflavin-S (ThioS) staining (Sigma, T1892), sections were dried at room temperature, rehydrated in PBS, and stained in 0.1% volume ThioS solution for 5 min at RT. Sections were then washed twice for 2 min each in 70% ethanol, washed again in PBS 1X, and then mounted in ProLong gold (Invitrogen, P36930). Images were acquired on a Nikon confocal microscope with z step set at 1 μm of thickness with a 10x air objective for evaluate immunoreactive areas and 60x oil objective for high resolution imaging of plaque associated microglia.

Three brain sections were analyzed for each animal. For each brain section, two regions of interest were imaged with base in their high amyloid levels: subiculum and somatosensory cortex. Images were analyzed using ImageJ (NIH). To determine immunoreactive area, Images were manually thresholded and maximum projections were prepared from z-stacks. Immunoreactive area was determined using the ‘measure’ function and averaged per area to determine the percentage of immunoreactive coverage. Aβ plaque counts were performed using the “analyze particles” function after manual threshold applied as mentioned above, and mask was applied to the images. For all applicable quantifications, physical area in square μm was determined using the ‘measure’ command of ImageJ for each region. Quantification is represented as either percent area coverage or count per square μm.

RNA isolation and quantitative real-time PCR—RNA was extracted from homogenized tissue using PureLink RNA Mini Columns following the manufacturer’s instructions. RNA was reverse transcribed into cDNA using the High-Capacity RNA to cDNA set. Taqman MasterMix and StepOne Plus (Applied Biosystems) was used for qPCR

as per the manufacturer's instructions. For all mRNA analyses, housekeeping gene GAPDH was used. Results are represented as relative fold change in gene expression normalized to the wild-type calibrator. For statistics, the relative delta Ct method was used.

Nanostring—The nCounter Analysis System (NanoString Technologies, Seattle, WA, USA) allows for multiplexed digital mRNA profiling without amplification or generation of cDNA[61]. Then nCounter Glial profiling panel profile 770 mouse genes across 50+ pathways involved in glial cell biology and quantify the relative abundance of 5 brain cell types and peripheral immune cells. Briefly, 200 ng of RNA was loaded for all samples and hybridized with probes for 16 h at 65 °C. Results obtained from nCounter MAX Analysis System (NanoString Technologies, catalog #NCT-SYST-LS, Seattle WA) were imported to Rosalind Analysis Platform (OnRamp Bioinformatics) for QC verification, normalization, and data statistics using Advanced Analysis (v2.0.115; NanoString Technologies). Probes were only included if the read count was more than 3 standard deviations above background, and probes that had <100 reads for 6 or more samples were removed from analysis. All assays were performed according to manufacturer protocols.

Western blot—After sonication, the soluble fraction of brain lysates was obtained by centrifugation for 10 min at 14,000 rpm. The protein samples were measured via Pierce BCA assay (Thermo-Fisher, 23225). For protein identification and relative quantification, 10 to 25 μg of proteins loaded onto Bolt 4%–12% Bis-Tris plus Protein gels (Thermo-Fisher, NW04122BOX) and run at 200 mV for 40 min. The proteins were then transferred onto PVDF membrane (Millipore, IPVH00010) at 400 mAmp for 90 min on ice. After 1 h of blocking in 5% BSA (in PBS 1X) the primary antibodies were then applied overnight in a blocking buffer at 4°C. The HRP-conjugated secondary antibodies were all incubated for 1h at RT at the proper dilution. The signal was developed using Immobilon western Chemiluminescent HRP Substrate (Millipore, WBKLS0500). Images were acquired with Amersham imager 600 (General-Electrics Healthcare) and protein quantification was performed by measuring the optical density of the specific bands with image J software (NIH). Samples from all experimental groups were loaded on each experiment and normalized to the respective control. For statistical analysis, normalized data across independent experiments were used together.

Cytokine panel assay—Mouse brain samples were assayed in duplicate using the MSD Proinflammatory Panel I (K15048D; MesoScale Discovery, Gaithersburg, MD, United States), a highly sensitive multiplex enzyme-linked immunosorbent assay (ELISA). This panel quantifies the following 10 proinflammatory cytokines in a single small sample volume (25 μL) of supernatant using an electrochemiluminescent detection method (MSD): interferon γ (IFN-γ), interleukin (IL)-1β, IL-2, IL-4, IL-6, IL-8, IL-10, IL-12p70, IL-13, and tumor necrosis factor α (TNFα). The mean intra-assay coefficient for each cytokine was <8.5%, based on the cytokine standards. Any value below the lower limit of detection (LLOD) for the cytokine assay was replaced with 1/2 LLOD of the assay for statistical analysis.

Flow cytometry—For *in vivo* phagocytosis evaluation, 3 hr before brain harvest, 5-month old mice were i.p. injected with a blood–brain barrier-penetrating Aβ dye, methoxy-XO4. If microglia are actively phagocytosing amyloid plaques, methoxy-XO4 will be internalized together with Aβ. Mice were perfused, brains removed, chopped, and digested using the Macs Neural tissue Dissociation kit (Miltenyl Biotec) and subsequent percoll gradients (30% percoll [GE healthcare], 10% fetal bovine serum) was used to purify myeloid cells and incubated to antibodies against Cd11b and CD45. Later, stained samples were fixed and permeabilized using the BD Cytofix/Cytoperm kit. Intracellular staining of HK2 was done by using a rabbit monoclonal antibody (Abcam) and an anti-rabbit conjugated secondary antibody. To evaluate microglial mitochondrial membrane potential (ΔΨM), we used Mitotracker deep red (DR). Samples were acquired on BD FACS Canto II (BD Bioscience) flow cytometer. Raw data were analyzed with FlowJo v10 (BD Bioscience). Cells were gated on $Cd11b^+$ and $Cd45^+$ to assess the level of HK2 expression, Aβ phagocytosis and ΔΨM as the geometric mean fluorescence intensity (gMFI).

Lonidamine quantification in mice brain and plasma—Brains and blood of Lonidamine treated mice were collected, weighed, crushed to a powder with mortar and pestle under liquid nitrogen, and powdered brains were stored at −80°C until analysis. A method to quantify Lonidamine from mouse brain and plasma has been developed using temazepam (TMP, Sigma) as the internal standard, liquid-liquid extraction, and HPLC-MS/MS (Sciex 5500 QTRAP). The mass spectrometer utilizes an electrospray ionization probe run in positive mode. The multiple reaction monitoring (MRM) Q1/Q3 (m/z) transitions for Lonidamine was 322.1/304.0 and temazepam is 301.1/255.0. The lower limit of quantification using 20 μL of mouse plasma was 3 ng/mL and for whole mouse brain was 2.4 ng/sample. The extraction uses phosphate buffer, pH 7.4, and methyl tertiary butyl ether. The mobile phase was delivered via gradient using acetonitrile and 0.1% formic acid on a Restek Ultra C18 50X4.6mm 5μm column.

Measurements of ATP levels, HK activity, and MTS assay—Primary microglia were seeded in a 96 well plate and after 24 hrs, cells were homogenized, and ATP, MTS (cell viability) and HK activity were measured using Luminescent ATP Detection Assay Kit (Abcam, ab113849), Colorimetric hexokinase activity assay kit (Abcam, ab136957) and CellTiter 96 Non-Radioactive Cell Proliferation Assay.

Dataset analysis—HK2 expression in GSE33000, dataset was analyzed using the online tool GEO2R (https://www.ncbi.nlm.nih.gov/geo/geo2r/).

QUANTIFICATION AND STATISTICAL ANALYSIS

Statistical tests, along with the number of animals analyzed, are indicated in the figure legends. Comparisons between two groups were conducted with the unpaired, two-tailed student’s t -tests or non-parametric Mann-Whitney test. Comparisons between multiple groups were conducted with the one-way ANOVA with Tukey’s post-hoc multiple comparison test using Prism 9 statistical software (GraphPad, San Diego, CA, United States). Error bars represent the standard error of the mean (SEM). Statistical significance was met when the p -value was less than 0.05.

Supplementary Material

Refer to Web version on PubMed Central for supplementary material.

ACKNOWLEDGMENTS

The authors would like to thank Dr. Nissim Hay from the Departments of Biochemistry and Molecular Genetics at the University of Illinois College of Medicine for his generous gift of the HK2 floxed mice. Lonidamine quantification was provided by the Clinical Pharmacology Analytical Core (CPAC) at Indiana University School of Medicine, supported by IU Simon Comprehensive Cancer Center support grant P30 CA082709.

This work was supported by a grant from the National Institutes of Health (to G.E.L., RF1AG068400). J.F.C. was supported by an Eli Lilly-Stark Neuroscience Research grant (EPAR1536) and the BrightFocus Foundation (A20201166F).

REFERENCES

1. Sasaki A, Yamaguchi H, Ogawa A, Sugihara S, and Nakazato Y. (1997). Microglial activation in early stages of amyloid beta protein deposition. Acta Neuropathol. 94, 316–322. 10.1007/s004010050713. [PubMed: 9341931]
2. Yuan P, Condello C, Keene CD, Wang Y, Bird TD, Paul SM, Luo W, Colonna M, Baddeley D, and Grutzendler J. (2016). TREM2 Haplodeficiency in Mice and Humans Impairs the Microglia Barrier Function Leading to Decreased Amyloid Compaction and Severe Axonal Dystrophy. Neuron 90, 724–739. 10.1016/j.neuron.2016.05.003. [PubMed: 27196974]
3. d'Errico P, Ziegler-Waldkirch S, Aires V, Hoffmann P, Mezö C, Erny D, Monasor LS, Liebscher S, Ravi VM, Joseph K, et al. (2022). Microglia contribute to the propagation of Aβ into unaffected brain tissue. Nat. Neurosci 25, 20–25. 10.1038/s41593-021-00951-0. [PubMed: 34811521]
4. Wang C, Fan L, Khawaja RR, Liu B, Zhan L, Kodama L, Chin M, Li Y, Le D, Zhou Y, et al. (2022). Microglial NF-κB drives tau spreading and toxicity in a mouse model of tauopathy. Nat. Commun 13, 1969. 10.1038/s41467-022-29552-6. [PubMed: 35413950]
5. Jain N, Lewis CA, Ulrich JD, and Holtzman DM (2023). Chronic TREM2 activation exacerbates Aβ-associated tau seeding and spreading. J. Exp. Med 220, e20220654. 10.1084/jem.20220654.
6. Ghosh S, Castillo E, Frias ES, and Swanson RA (2018). Bioenergetic regulation of microglia. Glia 66, 1200–1212. 10.1002/glia.23271. [PubMed: 29219210]
7. Loftus RM, and Finlay DK (2016). Immunometabolism: Cellular Metabolism Turns Immune Regulator. J. Biol. Chem 291, 1–10. 10.1074/jbc.R115.693903. [PubMed: 26534957]
8. Paolicelli RC, and Angiari S. (2019). Microglia immunometabolism: From metabolic disorders to single cell metabolism. Semin. Cell Dev. Biol 94, 129–137. 10.1016/j.semcdb.2019.03.012. [PubMed: 30954657]
9. Gimeno-Bayón J, López-López A, Rodríguez MJ, and Mahy N. (2014). Glucose pathways adaptation supports acquisition of activated microglia phenotype. J. Neurosci. Res 92, 723–731. 10.1002/jnr.23356. [PubMed: 24510633]
10. Pan R-Y, Ma J, Kong X-X, Wang X-F, Li S-S, Qi X-L, Yan Y-H, Cheng J, Liu Q, Jin W, et al. (2019). Sodium rutin ameliorates Alzheimer's disease–like pathology by enhancing microglial amyloid-β clearance. Sci. Adv 5, eaau6328. 10.1126/sciadv.aau6328.
11. Fairley LH, Wong JH, and Barron AM (2021). Mitochondrial Regulation of Microglial Immunometabolism in Alzheimer's Disease. Front. Immunol 12, 624538. 10.3389/fimmu.2021.624538.
12. Shen Y, Kapfhamer D, Minnella AM, Kim J-E, Won SJ, Chen Y, Huang Y, Low LH, Massa SM, and Swanson RA (2017). Bioenergetic state regulates innate inflammatory responses through the transcriptional co-repressor CtBP. Nat. Commun 8, 624. 10.1038/s41467-017-00707-0. [PubMed: 28935892]
13. Seki SM, and Gaultier A. (2017). Exploring Non-Metabolic Functions of Glycolytic Enzymes in Immunity. Front. Immunol 8, 1549. 10.3389/fimmu.2017.01549. [PubMed: 29213268]

14. De Jesus A, Keyhani-Nejad F, Pusec CM, Goodman L, Geier JA, Stoolman JS, Stanczyk PJ, Nguyen T, Xu K, Suresh KV, et al. (2022). Hexokinase 1 cellular localization regulates the metabolic fate of glucose. Mol. Cell 82, 1261–1277.e9. 10.1016/j.molcel.2022.02.028. [PubMed: 35305311]
15. Codocedo JF, and Landreth GE (2022). The intersection of metabolism and inflammation is governed by the intracellular topology of hexokinases and the metabolic fate of glucose. Immunometabolism 4, e00011. 10.1097/IN9.0000000000000011.
16. Granchi C, and Minutolo F. (2012). Anticancer Agents That Counteract Tumor Glycolysis. ChemMedChem 7, 1318–1350. 10.1002/cmdc.201200176. [PubMed: 22684868]
17. Baik SH, Ramanujan VK, Becker C, Fett S, Underhill DM, and Wolf AJ (2023). Hexokinase dissociation from mitochondria promotes oligomerization of VDAC that facilitates NLRP3 inflammasome assembly and activation. Sci. Immunol 8, eade7652. 10.1126/sciimmunol.ade7652.
18. Leng L, Yuan Z, Pan R, Su X, Wang H, Xue J, Zhuang K, Gao J, Chen Z, Lin H, et al. (2022). Microglial hexokinase 2 deficiency increases ATP generation through lipid metabolism leading to β-amyloid clearance. Nat. Metab 4, 1287–1305. 10.1038/s42255-022-00643-4. [PubMed: 36203054]
19. Hu Y, Cao K, Wang F, Wu W, Mai W, Qiu L, Luo Y, Ge W-P, Sun B, Shi L, et al. (2022). Dual roles of hexokinase 2 in shaping microglial function by gating glycolytic flux and mitochondrial activity. Nat. Metab 4, 1756–1774. 10.1038/s42255-022-00707-5. [PubMed: 36536134]
20. Cheng J, Zhang R, Xu Z, Ke Y, Sun R, Yang H, Zhang X, Zhen X, and Zheng L-T (2021). Early glycolytic reprogramming controls microglial inflammatory activation. J. Neuroinflammation 18, 129. 10.1186/s12974-021-02187-y. [PubMed: 34107997]
21. Wolf AJ, Reyes CN, Liang W, Becker C, Shimada K, Wheeler ML, Cho HC, Popescu NI, Coggeshall KM, Arditi M, and Underhill DM (2016). Hexokinase Is an Innate Immune Receptor for the Detection of Bacterial Peptidoglycan. Cell 166, 624–636. 10.1016/j.cell.2016.05.076. [PubMed: 27374331]
22. Sil A, Erfani A, Lamb N, Copland R, Riedel G, and Platt B. (2022). Sex Differences in Behavior and Molecular Pathology in the 5XFAD Model.J. Alzheimers Dis. 85, 755–778. 10.3233/JAD-210523.
23. Casali BT, MacPherson KP, Reed-Geaghan EG, and Landreth GE (2020). Microglia depletion rapidly and reversibly alters amyloid pathology by modification of plaque compaction and morphologies. Neurobiol. Dis 142, 104956. 10.1016/j.nbd.2020.104956.
24. Keren-Shaul H, Spinrad A, Weiner A, Matcovitch-Natan O, Dvir-Szternfeld R, Ulland TK, David E, Baruch K, Lara-Astaiso D, Toth B, et al. (2017). A Unique Microglia Type Associated with Restricting Development of Alzheimer's Disease. Cell 169, 1276–1290.e17. 10.1016/j.cell.2017.05.018. [PubMed: 28602351]
25. Krasemann S, Madore C, Cialic R, Baufeld C, Calcagno N, El Fatimy R, Beckers L, O'Loughlin E, Xu Y, Fanek Z, et al. (2017). The TREM2-APOE Pathway Drives the Transcriptional Phenotype of Dysfunctional Microglia in Neurodegenerative Diseases. Immunity 47, 566–581.e9. 10.1016/j.immuni.2017.08.008. [PubMed: 28930663]
26. Morgan BP (2018). Complement in the pathogenesis of Alzheimer's disease. Semin. Immunopathol 40, 113–124. 10.1007/s00281-017-0662-9. [PubMed: 29134267]
27. De Schepper S, Ge JZ, Crowley G, Ferreira LSS, Garceau D, Toomey CE, Sokolova D, Rueda-Carrasco J, Shin S-H, Kim J-S, et al. (2023). Perivascular cells induce microglial phagocytic states and synaptic engulfment via SPP1 in mouse models of Alzheimer's disease. Nat. Neurosci 26, 406–415. 10.1038/s41593-023-01257-z. [PubMed: 36747024]
28. Liu S, Liu Y, Hao W, Wolf L, Kiliaan AJ, Penke B, Ru€be CE, Walter J, Heneka MT, Hartmann T, et al. (2012). TLR2 is a primary receptor for Alzheimer's amyloid β peptide to trigger neuroinflammatory activation. J. Immunol 188, 1098–1107. 10.4049/jimmunol.1101121. [PubMed: 22198949]
29. Guillot-Sestier M-V, Araiz AR, Mela V, Gaban AS, O'Neill E, Joshi L, Chouchani ET, Mills EL, and Lynch MA (2021). Microglial metabolism is a pivotal factor in sexual dimorphism in Alzheimer's disease. Commun. Biol 4, 711. 10.1038/s42003-021-02259-y. [PubMed: 34112929]

30. Lynch MA (2022). Exploring Sex-Related Differences in Microglia May Be a Game-Changer in Precision Medicine. Front. Aging Neurosci. 14, 868448. 10.3389/fnagi.2022.868448.

31. Patra KC, Wang Q, Bhaskar PT, Miller L, Wang Z, Wheaton W, Chandel N, Laakso M, Muller WJ, Allen EL, et al. (2013). Hexokinase 2 is required for tumor initiation and maintenance and its systemic deletion is therapeutic in mouse models of cancer. Cancer Cell 24, 213–228. 10.1016/j.ccr.2013.06.014. [PubMed: 23911236]

32. Oakley H, Cole SL, Logan S, Maus E, Shao P, Craft J, Guillozet-Bongaarts A, Ohno M, Disterhoft J, Van Eldik L, et al. (2006). Intraneuronal beta-amyloid aggregates, neurodegeneration, and neuron loss in transgenic mice with five familial Alzheimer's disease mutations: potential factors in amyloid plaque formation. J. Neurosci 26, 10129–10140. 10.1523/JNEUROSCI.1202-06.2006. [PubMed: 17021169]

33. Faust TE, Feinberg PA, O'Connor C, Kawaguchi R, Chan A, Strasburger H, Frosch M, Boyle MA, Masuda T, Amann L, et al. (2023). A comparative analysis of microglial inducible Cre lines. Cell Rep. 42, 113031. 10.1016/j.celrep.2023.113031.

34. Schoch KM, Ezerskiy LA, Morhaus MM, Bannon RN, Sauerbeck AD, Shabsovich M, Jafar-Nejad P, Rigo F, and Miller TM (2021). Acute Trem2 reduction triggers increased microglial phagocytosis, slowing amyloid deposition in mice. Proc. Natl. Acad. Sci. USA 118, e2100356118. 10.1073/pnas.2100356118.

35. Meilandt WJ, Ngu H, Gogineni A, Lalehzadeh G, Lee S-H, Srinivasan K, Imperio J, Wu T, Weber M, Kruse AJ, et al. (2020). Trem2 Deletion Reduces Late-Stage Amyloid Plaque Accumulation, Elevates the Aβ42:Aβ40 Ratio, and Exacerbates Axonal Dystrophy and Dendritic Spine Loss in the PS2APP Alzheimer's Mouse Model. J. Neurosci 40, 1956–1974. 10.1523/JNEUROSCI.1871-19.2019. [PubMed: 31980586]

36. Wolf A, Bauer B, Abner EL, Ashkenazy-Frolinger T, and Hartz AMS (2016). A Comprehensive Behavioral Test Battery to Assess Learning and Memory in 129S6/Tg2576 Mice. PLoS One 11, e0147733. 10.1371/journal.pone.0147733.

37. Garcia SN, Guedes RC, and Marques MM (2019). Unlocking the potential of HK2 in cancer metabolism and therapeutics. Curr. Med. Chem 26, 7285–7322. 10.2174/0929867326666181213092652. [PubMed: 30543165]

38. Cervantes-Madrid D, Romero Y, and Dueñas-González A. (2015). Reviving Lonidamine and 6-Diazo-5-oxo-L-norleucine to Be Used in Combination for Metabolic Cancer Therapy. BioMed Res. Int 2015, 690492. 10.1155/2015/690492.

39. Huang Y, Sun G, Sun X, Li F, Zhao L, Zhong R, and Peng Y. (2020). The Potential of Lonidamine in Combination with Chemotherapy and Physical Therapy in Cancer Treatment. Cancers 12, 3332. 10.3390/cancers12113332. [PubMed: 33187214]

40. Feng W, Zhang Y, Wang Z, Xu H, Wu T, Marshall C, Gao J, and Xiao M. (2020). Microglia prevent beta-amyloid plaque formation in the early stage of an Alzheimer's disease mouse model with suppression of glymphatic clearance. Alzheimer's Res. Ther 12, 125. 10.1186/s13195-020-00688-1. [PubMed: 33008458]

41. Thawkar BS, and Kaur G. (2019). Inhibitors of NF-κB and P2X7/NLRP3/Caspase 1 pathway in microglia: Novel therapeutic opportunities in neuroinflammation induced early-stage Alzheimer's disease. J. Neuroimmunol 326, 62–74. 10.1016/j.jneuroim.2018.11.010. [PubMed: 30502599]

42. Oblak AL, Lin PB, Kotredes KP, Pandey RS, Garceau D, Williams HM, Uyar A, O'Rourke R, O'Rourke S, Ingraham C, et al. (2021). Comprehensive Evaluation of the 5XFAD Mouse Model for Preclinical Testing Applications: A MODEL-AD Study. Front. Aging Neurosci. 13, 713726. 10.3389/fnagi.2021.713726.

43. Bianco A, Antonacci Y, and Liguori M. (2023). Sex and Gender Differences in Neurodegenerative Diseases: Challenges for Therapeutic Opportunities. Int. J. Mol. Sci 24, 6354. 10.3390/ijms24076354. [PubMed: 37047320]

44. Zucker I, and Prendergast BJ (2020). Sex differences in pharmacokinetics predict adverse drug reactions in women. Biol. Sex Differ. 11, 32. 10.1186/s13293-020-00308-5. [PubMed: 32503637]

45. Nath K, Guo L, Nancolas B, Nelson DS, Shestov AA, Lee S-C, Roman J, Zhou R, Leeper DB, Halestrap AP, et al. (2016). Mechanism of antineoplastic activity of lonidamine. Biochim. Biophys. Acta 1866, 151–162. 10.1016/j.bbcan.2016.08.001. [PubMed: 27497601]

46. Bhutia YD, Babu E, and Ganapathy V. (2016). Re-programming tumour cell metabolism to treat cancer: no lone target for lonidamine. Biochem. J 473, 1503–1506. 10.1042/BCJ20160068. [PubMed: 27234586]
47. Wang P, Henning SM, and Heber D. (2010). Limitations of MTT and MTS-based assays for measurement of antiproliferative activity of green tea polyphenols. PLoS One 5, e10202. 10.1371/journal.pone.0010202.
48. Gao C, Jiang J, Tan Y, and Chen S. (2023). Microglia in neurodegenerative diseases: mechanism and potential therapeutic targets. Signal Transduct. Targeted Ther. 8, 359. 10.1038/s41392-023-01588-0.
49. Venegas C, Kumar S, Franklin BS, Dierkes T, Brinkschulte R, Tejera D, Vieira-Saecker A, Schwartz S, Santarelli F, Kummer MP, et al. (2017). Microglia-derived ASC specks cross-seed amyloid-β in Alzheimer's disease. Nature 552, 355–361. 10.1038/nature25158. [PubMed: 29293211]
50. Zipp F, Bittner S, and Schafer DP (2023). Cytokines as emerging regulators of central nervous system synapses. Immunity 56, 914–925. 10.1016/j.immuni.2023.04.011. [PubMed: 37163992]
51. Guo D, Tong Y, Jiang X, Meng Y, Jiang H, Du L, Wu Q, Li S, Luo S, Li M, et al. (2022). Aerobic glycolysis promotes tumor immune evasion by hexokinase2-mediated phosphorylation of IKBα. Cell Metabol. 34, 1312–1324.e6. 10.1016/j.cmet.2022.08.002.
52. Demarquoy J, and Le Borgne F. (2015). Crosstalk between mitochondria and peroxisomes. World J. Biol. Chem 6, 301–309. 10.4331/wjbc.v6.i4.301. [PubMed: 26629313]
53. Lin J, Fang W, Xiang Z, Wang Q, Cheng H, Chen S, Fang J, Liu J, Wang Q, Lu Z, and Ma L. (2023). Glycolytic enzyme HK2 promotes PD-L1 expression and breast cancer cell immune evasion. Front. Immunol 14, 1189953. 10.3389/fimmu.2023.1189953.
54. Baik SH, Kang S, Lee W, Choi H, Chung S, Kim J-I, and Mook-Jung I. (2019). A Breakdown in Metabolic Reprogramming Causes Microglia Dysfunction in Alzheimer's Disease. Cell Metabol. 30, 493–507.e6. 10.1016/j.cmet.2019.06.005.
55. Lynch MA (2020). Can the emerging field of immunometabolism provide insights into neuroinflammation? Prog. Neurobiol 184, 101719. 10.1016/j.pneurobio.2019.101719.
56. Vilalta A, and Brown GC (2014). Deoxyglucose prevents neurodegeneration in culture by eliminating microglia. J. Neuroinflammation 11, 58. 10.1186/1742-2094-11-58. [PubMed: 24669778]
57. Hinrichsen F, Hamm J, Westermann M, Schröder L, Shima K, Mishra N, Walker A, Sommer N, Klischies K, Prasse D, et al. (2021). Microbial regulation of hexokinase 2 links mitochondrial metabolism and cell death in colitis. Cell Metabol. 33, 2355–2366.e8. 10.1016/j.cmet.2021.11.004.
58. Sayed FA, Telpoukhovskaia M, Kodama L, Li Y, Zhou Y, Le D, Hauduc A, Ludwig C, Gao F, Clelland C, et al. (2018). Differential effects of partial and complete loss of TREM2 on microglial injury response and tauopathy. Proc. Natl. Acad. Sci. USA 115, 10172–10177. 10.1073/pnas.1811411115. [PubMed: 30232263]
59. Andreone BJ, Przybyla L, Llapashtica C, Rana A, Davis SS, van Lengerich B, Lin K, Shi J, Mei Y, Astarita G, et al. (2020). Alzheimer's-associated PLCγ2 is a signaling node required for both TREM2 function and the inflammatory response in human microglia. Nat. Neurosci 23, 927–938. 10.1038/s41593-020-0650-6. [PubMed: 32514138]
60. Narayanan M, Huynh JL, Wang K, Yang X, Yoo S, McElwee J, Zhang B, Zhang C, Lamb JR, Xie T, et al. (2014). Common dysregulation network in the human prefrontal cortex underlies two neurodegenerative diseases. Mol. Syst. Biol 10, 743. 10.15252/msb.20145304. [PubMed: 25080494]
61. Geiss GK, Bumgarner RE, Birditt B, Dahl T, Dowidar N, Dunaway DL, Fell HP, Ferree S, George RD, Grogan T, et al. (2008). Direct multiplexed measurement of gene expression with color-coded probe pairs. Nat. Biotechnol 26, 317–325. 10.1038/nbt1385. [PubMed: 18278033]

Highlights

- Hexokinase 2, the first enzyme of glycolysis, is upregulated in Aβ plaque-associated microglia
- Partial and complete loss of microglial HK2 induces differential effects on AD progression
- HK2 deletion is associated with mitochondrial dysfunction and inflammation in microglia
- HK2 partial antagonism targets the IKBα-NF-κB microglial pathway to exert beneficial effects

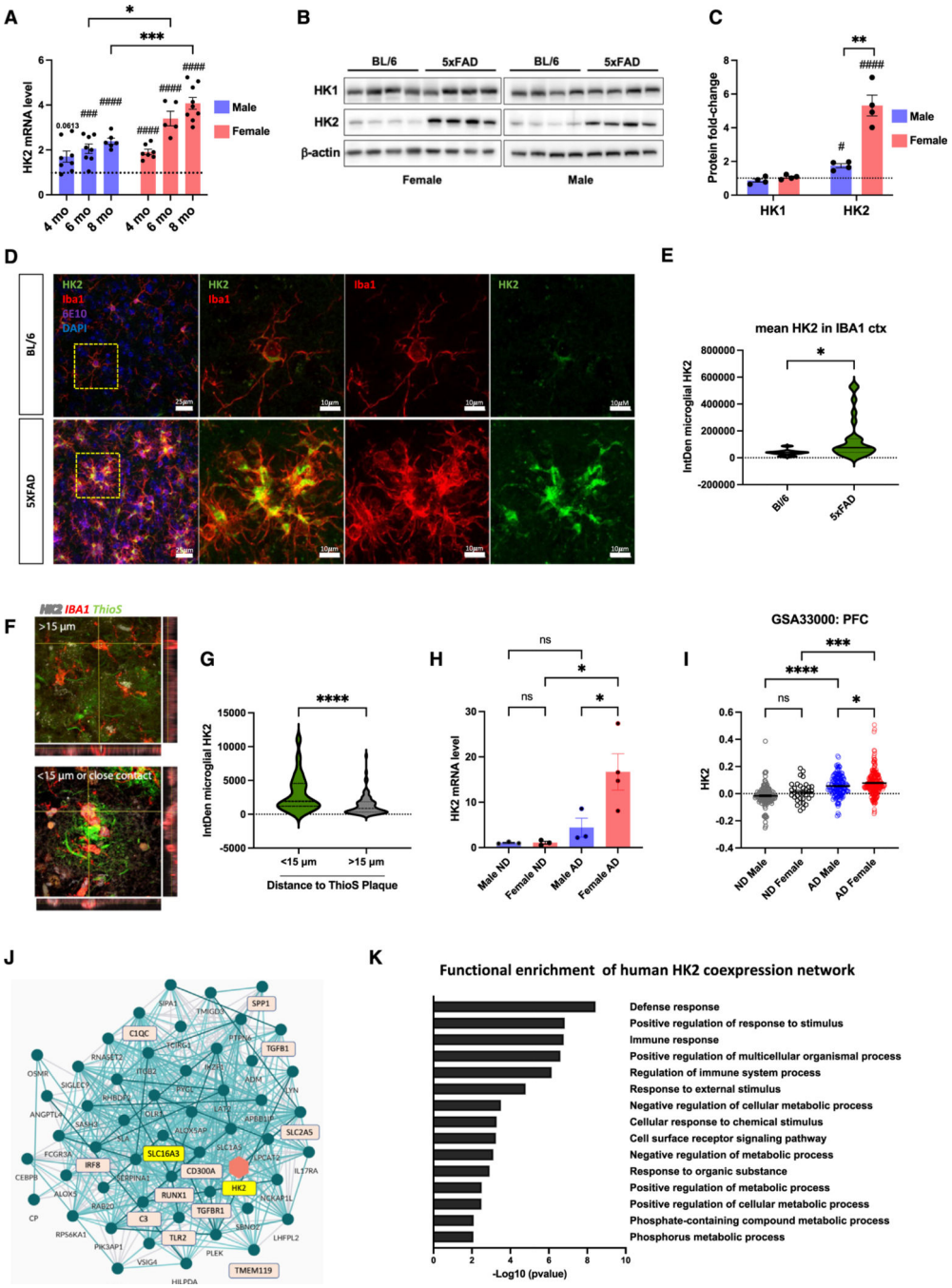

Figure 1. HK2 as a molecular hub between metabolism and immune response in AD

(A) qPCR analysis of HK2 expression during disease progression in the cortex of male and female 5xFAD mice. The dashed line represents gene expression in BL/6 control mice. Unpaired t test analysis revealed significant genotype-related increases ($^{###}p < 0.001$, $^{####}p < 0.0001$) and a significant increase in HK2 expression in the cortex of females compared with male 5xFAD mice at 6 and 8 months ($^{*}p < 0.05$, $^{***}p < 0.001$, $n = 5–9$ per group, two-way ANOVA followed by Sidak's multiple comparisons test).

(B and C) Western blot and quantification of HK1 and HK2 in the 8-month-old 5xFAD mouse cortex. The dashed line represents gene expression in BL/6 control mice. Densitometric analysis of hexokinase isoforms was normalized to β-actin levels ($n = 4$, genotype difference, $^{\#}p < 0.05$, $^{\#\#\#\#}p < 0.0001$, and sex difference, $^{**}p < 0.01$; unpaired t test).

(D) Confocal images of microglial HK2 expression in the cortex of 8-month-old BL/6 (top) and 5xFAD mice (bottom). Scale bar: 25 μm. Yellow box: zoomed images of resting and Aβ-plaque (6E10, purple)-associated microglia ($Iba1^+$, red) expressing HK2 (green). Scale bar: 10 μm.

(E) Quantification of the integrated density of HK2 in $Iba1^+$ cells. After the binarization of the Iba1-immunoreactive signal, the mean fluorescence intensity of HK2 was calculated and multiplied by the area of Iba1. $^{*}p < 0.05$ ($n = 50$ cells, from five mice per group; unpaired t test).

(F) Immunofluorescent staining of HK2 (white), Iba1 (red), and ThioS (green) of brain samples of AD patients.

(G) Quantification of the integrated density of HK2 in $Iba1^+$ cells in close contact with Aβ (in radius <15 μm from Aβ) and away from Aβ (>15 μm). $^{****}p < 0.0001$ ($n = 50–77$ cells per group, from two healthy and three AD patients, respectively; unpaired t test).

(H) qPCR analysis of HK2 expression in female vs. male postmortem samples of non-demented (ND) and AD patients normalized to the expression of $Iba1^+$ ($n = 3–4$).

(I) HK2 expression obtained from a human transcriptomic dataset of prefrontal cortex tissue (PFC) of 157 non-demented controls and 310 AD patients (GSE33000). Data segregated by sex reveal a significant difference in the upregulated levels of HK2 between women and men.

(J) AMP-AD consortium co-expression network analysis of RNA-seq data from AD cases and controls. The HK2 node is highlighted in yellow, and co-expressed genes associated with microglial activation or identity are highlighted in pink. The network analysis performed by the AMP-AD consortium uses an ensemble methodology to identify genes that show similar co-expression across individuals.

(K) Gene ontology of HK2 co-expression network. The list of specific microglial genes co-expressed with HK2 in hAD cases was used to evaluate the top 15 biological processes associated with its expression.

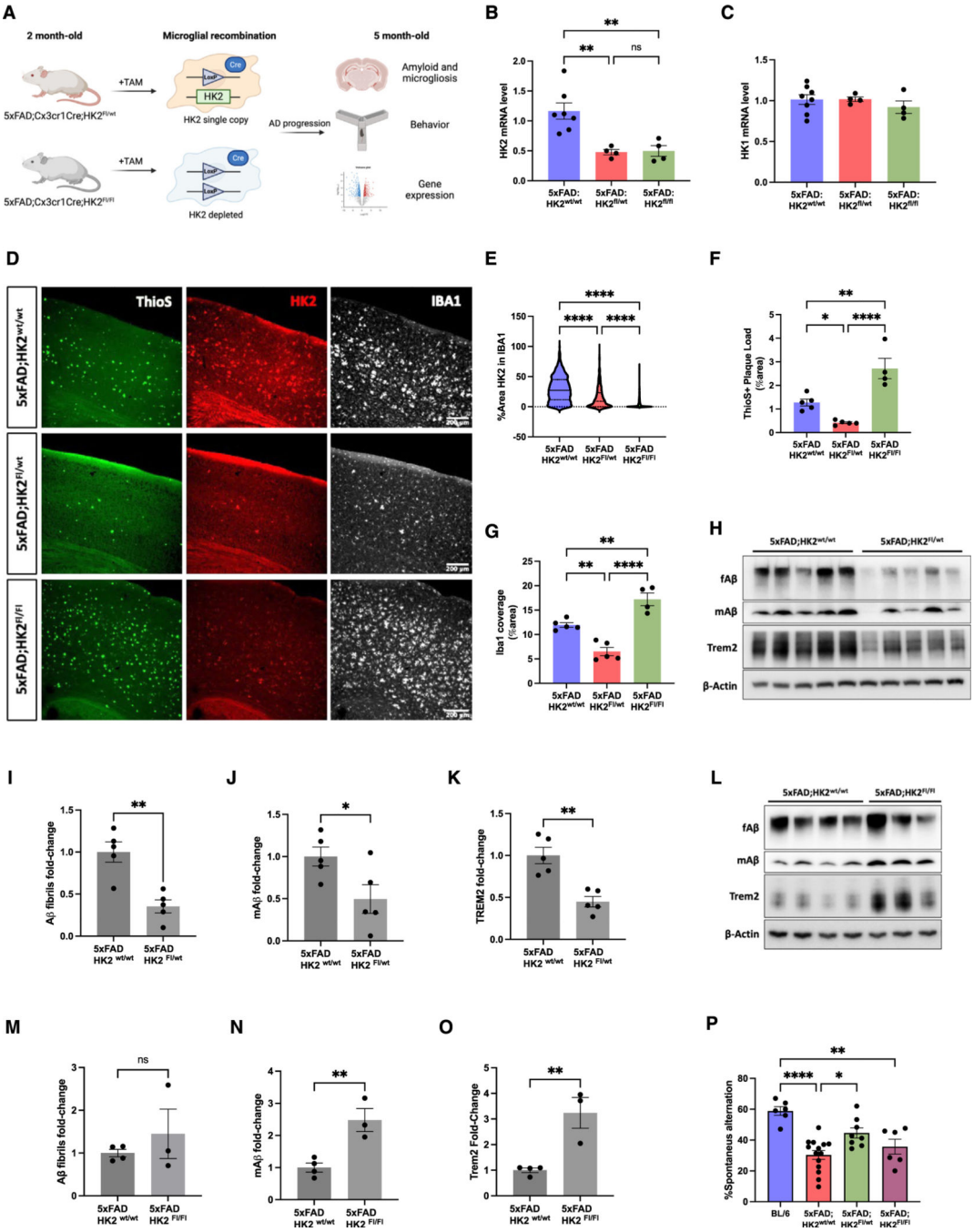

Figure 2. Gene dosage of microglial HK2 selectively modulates disease progression in the 5xFAD mice

(A) Mice with a conditional deletion of one or two copies of the HK2 gene in microglial cells were generated by crossing 5xFAD; CX3CR1-CreERT2 mice with mice harboring floxed HK2 alleles. At 2 months, five i.p. injections of TAM were administered to induce recombination. Mice were assessed at 5 months of age.

(B and C) qPCR analysis of HK2 and HK1 expression in the cortex of 5xFAD mice harboring two ($HK2^{WT/WT}$), one ($HK2^{Fl/WT}$), or no copies ($HK2^{Fl/Fl}$) of the HK2 gene. $^{**}p < 0.01$, $^{*}p < 0.05$ ($n = 4$–7 per group, one-way ANOVA followed by Tukey's *post hoc* test).

(D–G) Immunofluorescence analysis (D) of HK2 (red), microglia (Iba1, white), and Aβ (ThioS, green) in the cortical region of control and HK2-deficient mice. (E) Quantification of the percentage of microglial area containing HK2 immunoreactivity shown in (D); n = 12 slices from four or five mice. (F and G) Quantification of cortical area fraction of ThioS (plaque load) and microglia ($Iba1^+$ cells). *$p < 0.05$, **$p < 0.01$, ****$p < 0.0001$ (n = 4–5 per group, one-way ANOVA followed by Tukey's *post hoc* test).

(H) Representative immunoblots of fibrillar and monomeric Aβ detected by MOAB2 antibody and Trem2 from the soluble fraction of cortical lysates of 5xFAD; $HK2^{WT/WT}$ and 5xFAD; $HK2^{Fl/WT}$ mice treated with TAM.

(I–K) Immunoreactive bands were quantified, normalized to β-actin, and expressed as the fold change with respect to 5xFAD; $HK2^{WT/WT}$ mice. *$p < 0.05$ and **$p < 0.01$ (n = 5, unpaired t test).

(L) Representative immunoblots of fibrillar and monomeric Aβ detected by MOAB2 antibody and Trem2 from the soluble fraction of cortical lysates of 5xFAD; $HK2^{WT/WT}$ and 5xFAD; $HK2^{Fl/Fl}$ mice treated with TAM.

(M–O) Immunoreactive bands were quantified, normalized to β-actin, and expressed as the fold change with respect to 5xFAD; $HK2^{WT/WT}$ mice. *$p < 0.05$ and **$p < 0.01$ (n = 3–4 per group, unpaired t test).

(P) Percentage of spontaneous alternation behavior in a Y maze to evaluate spatial working memory (n = 6–14 per group, one-way ANOVA followed by Tukey's *post hoc* test).

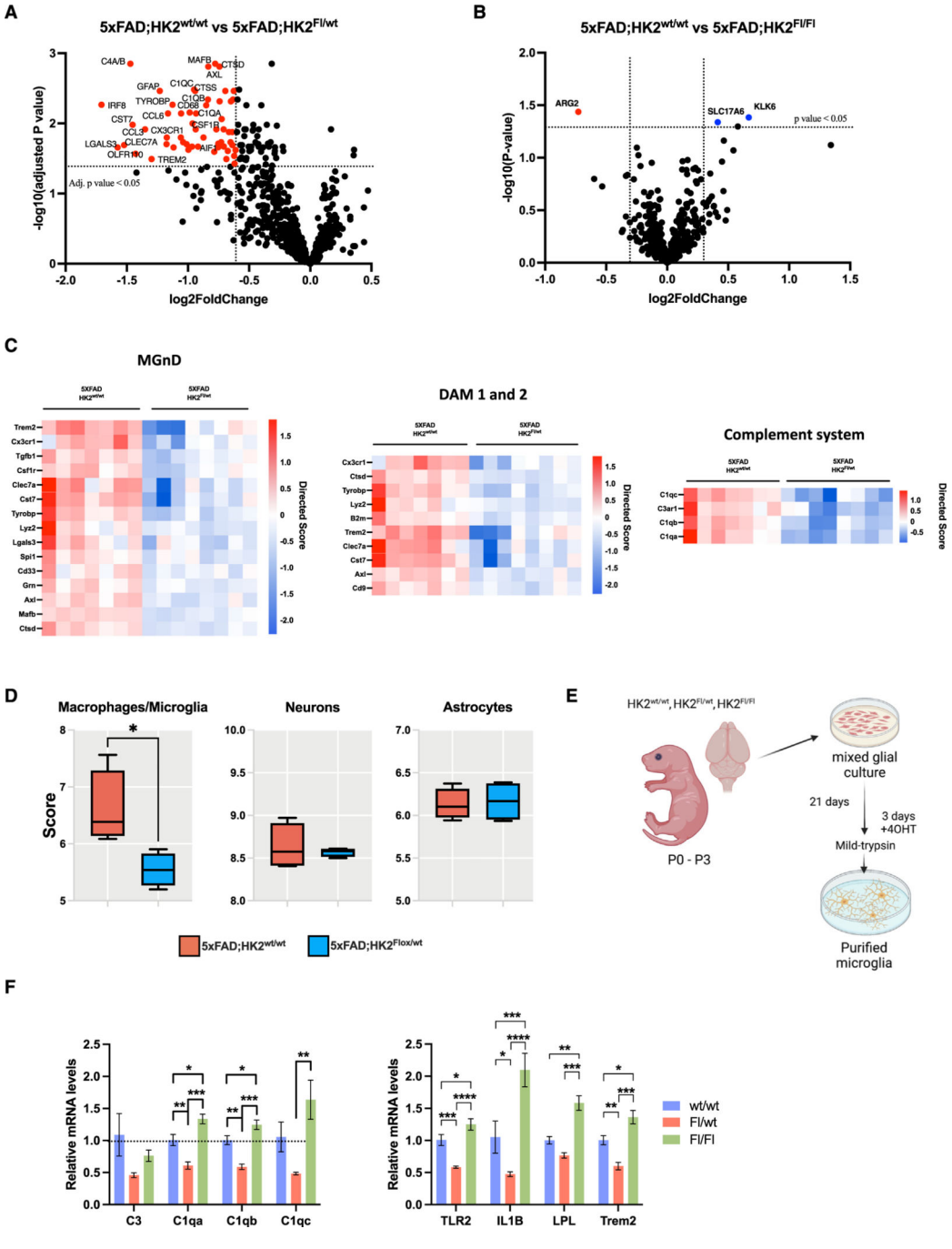

Figure 3. Gene dosage of microglial HK2 selectively modulates microglial gene expression in the 5xFAD mice

(A and B) Effect of HK2 gene dosage on gene expression with respect to 5xFAD; $HK2^{WT/WT}$ control mice. Differences for 770 genes in the NanoString glia panel are expressed as volcano plots. Adjusted *p* values were obtained from Rosalind using ramp software. Significance set at adj-$p < 0.05$ and fold change >1.5 and < −1.5 ($n = 7–8$).

(C) Heatmaps depicting the directed significance scores for genes annotated as markers of neurodegenerative phenotype (MGnD), DAM signature, and the complement system. The score magnitude of these gene sets was reduced only in the HK2-haploinsufficient AD mice.

(D) Cell abundance scores reveal a microglial-specific effect of HK2 partial loss. Cell type scores are based on the NanoString Cell Type Profiling Module; *$p < 0.05$ ($n = 5$, Mann-Whitney test).

(E) Schematic of the experimental procedure for analyzing primary cultures of microglia. 4-OHT, 4-hydroxytamoxifen.

(F) qPCR analysis of selected microglial genes in primary cultures of HK2-deficient microglia. *$p < 0.05$, **$p < 0.01$, ***$p < 0.001$, ****$p < 0.0001$ ($n = 4$–5 per group, one-way ANOVA followed by Tukey's *post hoc* test).

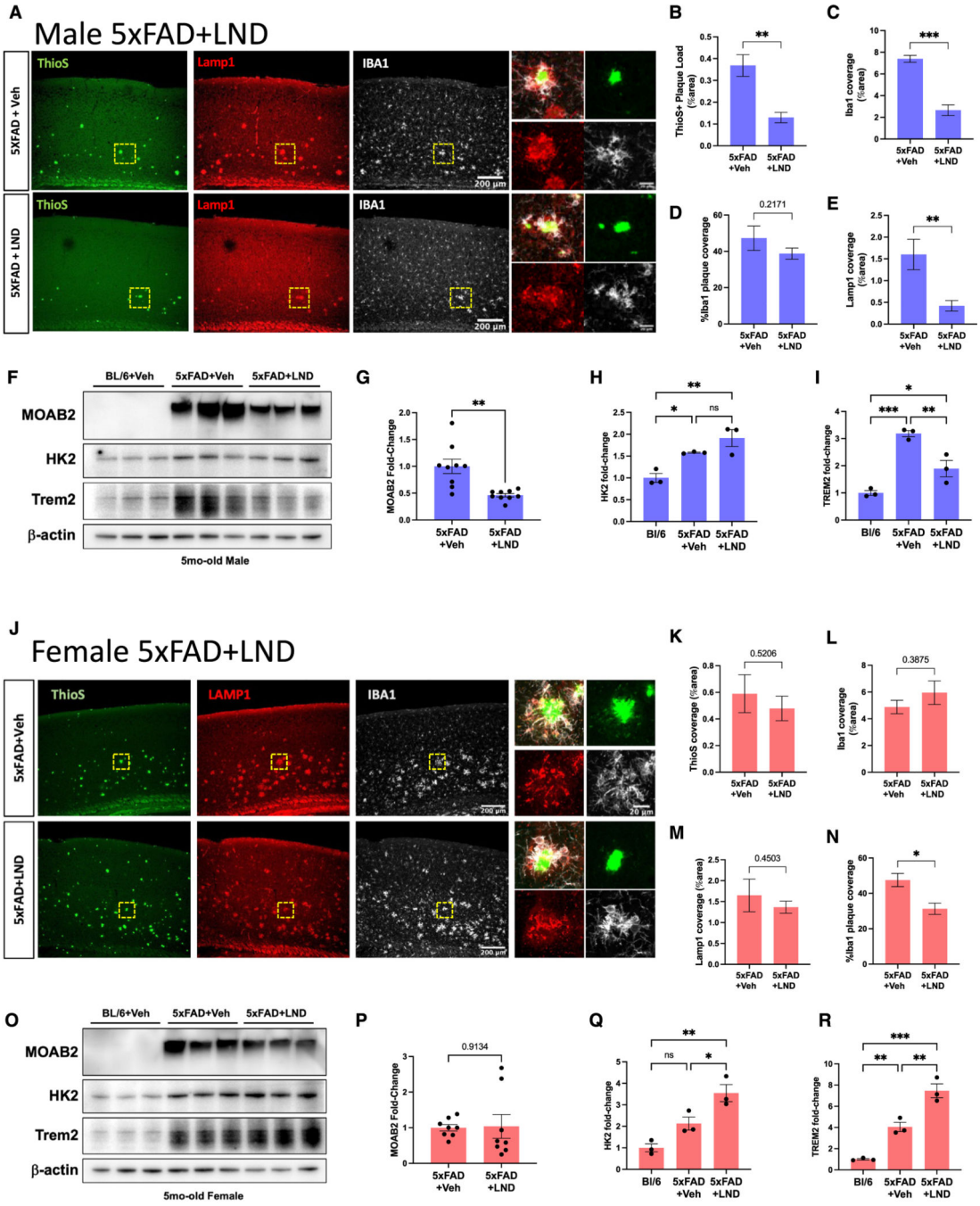

Figure 4. HK2 inhibition with lonidamine modulates amyloid pathology in a sex-dependent manner

(A) Immunohistochemical analysis of the cortical region of 5-month-old 5xFAD male mice treated with LND or vehicle. Amyloid plaques were stained with ThioS (green), dystrophic neurites with Lamp1 (red), and microglia with Iba1 (white). The dashed square area was magnified to better visualize microglial plaque coverage and the Lamp1 area (right). (B–E) Quantification of cortical area fraction of ThioS (B), Iba1 (C), and Lamp1 (D). (E) Microglial plaque coverage was evaluated by quantifying the average percentage area of

Iba1 in individual ThioS plaques across the whole cortex (n = 8–10 per group, unpaired t test).

(F–I) Western blot and quantification of proteins from the soluble fraction of cortical lysates of BL/6 and 5xFAD male mice treated with vehicle or LND. (F) Representative immunoblots of fibrillar Aβ detected with MOAB2 antibody and microglial proteins HK2 and Trem2. (G and H) Immunoreactive bands were quantified, normalized to β-actin, and expressed as the percentage of 5xFAD +Veh mice in the case of MOAB2. $^{**}p < 0.01$ (n = 9, unpaired t test). For the other proteins, the values are expressed as the percentage of BL/6 +Veh mice ($^{*}p < 0.05$, $^{**}p < 0.01$, $^{***}p < 0.001$; n = 3, one-way ANOVA, Tukey's posttest).

(J) Immunohistochemical analysis of the cortical region of 5-month-old 5xFAD female mice treated with LND or vehicle. Amyloid plaques were stained with ThioS (green), dystrophic neurites with Lamp1 (red), and microglia with Iba1 (white). The dashed square area was magnified to better visualize microglial plaque coverage and the Lamp1 area (right).

(K–N) Quantification of cortical area fraction of ThioS (K), Iba1 (L), and Lamp1 (M). (N) Microglial plaque coverage was evaluated by quantifying the average percentage area of Iba1 in individual ThioS plaques across the whole cortex (n = 8–10 per group, unpaired t test).

(O–R) Western blot and quantification of proteins from the soluble fraction of cortical lysates of BL/6 and 5xFAD male mice treated with vehicle or LND. (O) Representative immunoblots of fibrillar Aβ detected with MOAB2 antibody and microglial proteins HK2 and Trem2. (P–R) Immunoreactive bands were quantified, normalized to β-actin, and expressed as the percentage of 5xFAD +Veh mice in the case of MOAB2 (n = 8, unpaired t test). For the other proteins, the values are expressed as the percentage of BL/6 +Veh mice ($^{*}p < 0.05$, $^{**}p < 0.01$, $^{***}p < 0.001$; n = 3, one-way ANOVA, Tukey's posttest).

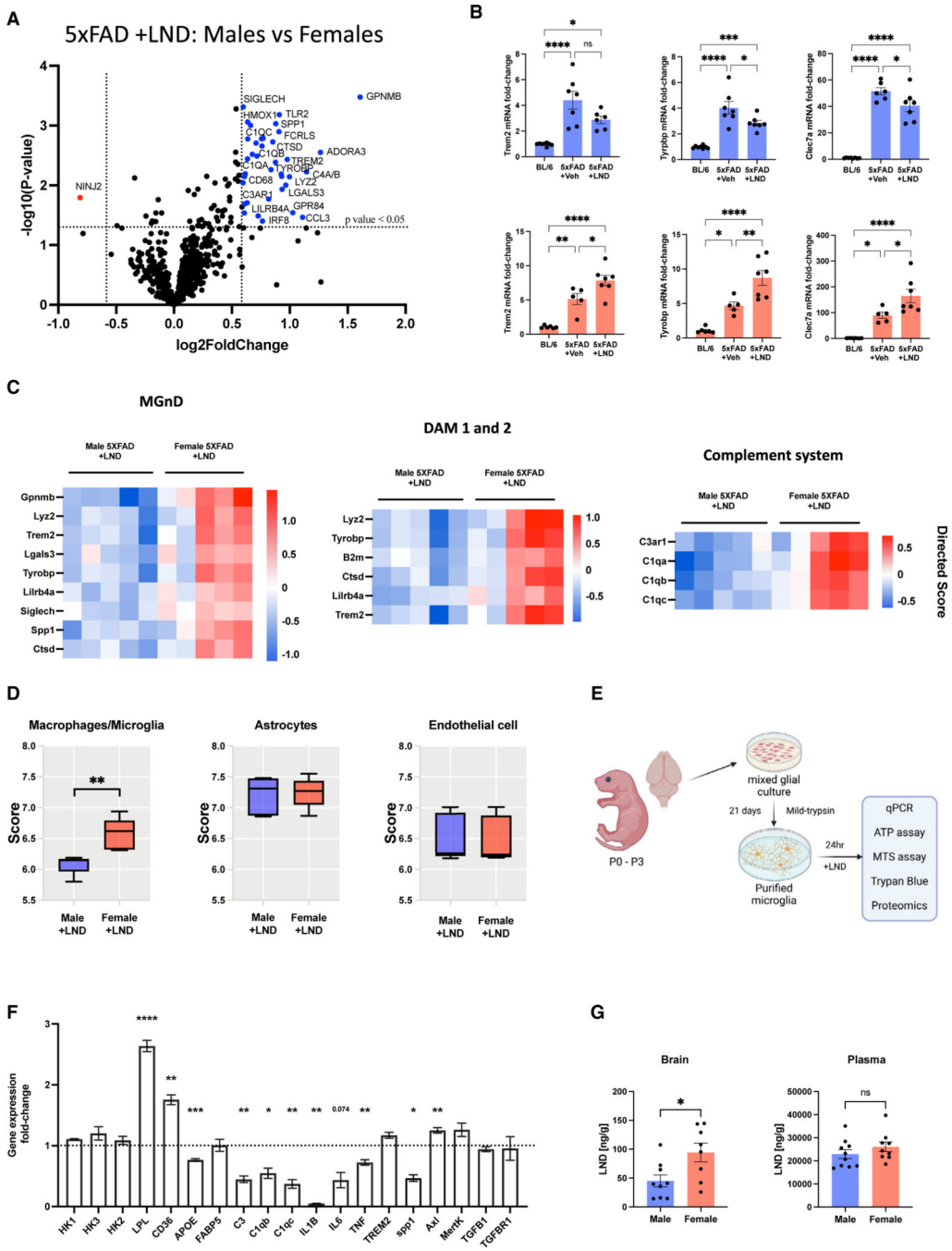

Figure 5. LND regulates the neuroinflammatory activation of microglia in a sex-dependent manner

(A) Volcano plot illustrating the statistical significance of sex-related differences in gene expression after treatment with LND in 5xFAD mice. Significance set at $p < 0.05$ and fold change <1.5 ($n = 5$ per group).

(B) qPCR analysis of selected microglial genes in the cortex of male (top, blue graphs) and female (bottom, salmon graphs) 5xFAD mice treated with LND. *$p < 0.05$, **$p < 0.01$, ***$p < 0.001$, $p < 0.0001$ ($n = 5$–8 per group, one-way ANOVA, Tukey's posttest).

(C) Heatmaps depicting the global significance scores for NanoString annotated pathways. GSEA revealed multiple immune-associated pathways upregulated in the female cortex of 5-month-old mice treated with LND compared to male treated mice.
(D) Cell type abundance scores based on the NanoString Cell Type Profiling Module. $^{**}p < 0.01$ ($n = 5$ per group, Mann-Whitney test).
(E) Schematic of the experimental procedure for analyzing primary cultures of microglia treated with LND.
(F) qPCR analysis of selected microglial genes in primary cultures of microglia treated with LND. $^{*}p < 0.05$, $^{**}p < 0.01$, $^{***}p < 0.001$ ($n = 3$ per group, unpaired t test). The dashed line represents gene expression in vehicle-treated cultures.
(G) Lonidamine brain and plasma levels were evaluated by HPLC after 4 h of a single i.p. injection. $^{*}p < 0.05$ ($n = 8$ or 9 per group, unpaired t test).

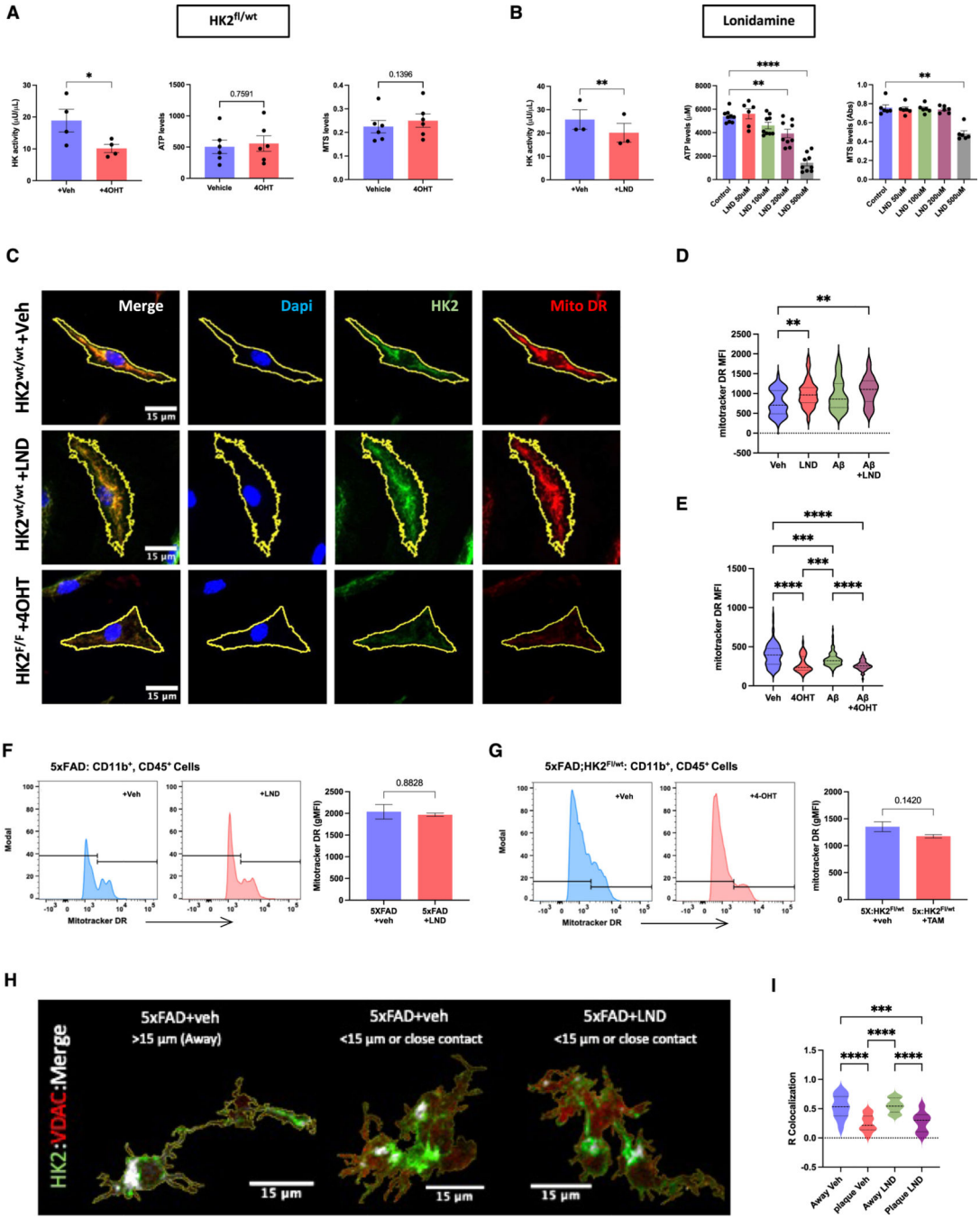

Figure 6. HK2 inhibition reduces cellular ATP levels, and its gene dosage induces divergent effects on mitochondrial function

(A) *In vitro* evaluation of HK activity, ATP levels, and cellular metabolism in primary cultures of microglia haploinsufficient for HK2 (*$p < 0.05$, $n = 4–6$ per group, unpaired t test).

(B) *In vitro* evaluation of HK activity, ATP levels, and cellular metabolism in primary cultures of microglia treated with different concentrations of the HK2 inhibitor LND (**$p < 0.01$, $n = 3$ per group, unpaired t test, and **$p < 0.01$, ****$p < 0.0001$, $n = 9$ per group, one-way ANOVA, Tukey's posttest, respectively).

(C) Representative confocal microscopy images showing MitoTracker DR staining (red) in primary cultures of microglia incubated with aggregated Aβ 1–42 for 24 h. Cells were co-incubated with vehicle (top), LND (middle), or 4-OHT (bottom) to antagonize HK2 (green). DAPI stain was used to visualize nuclei. Scale bar: 15 μm.

(D and E) Quantification of the mean fluorescence intensity (MFI) of MitoTracker DR in primary microglia described in (C). $^{**}p < 0.01$, $^{***}p < 0.001$, $^{****}p < 0.0001$ ($n = 33–70$ cells per group, from four independent experiments, one-way ANOVA, Tukey's posttest).

(F) Flow cytometry analysis of mitochondrial potential in $CD11b^+$, $CD45^+$ cells treated with LND. Left: representative histogram of the fluorescence intensity of MitoTracker deep red (DR) in microglia from 5xFAD mice treated with vehicle or LND. Right: quantification of the geometric MFI (gMFI) of MitoTracker DR ($n = 3$ per group, unpaired t test).

(G) Flow cytometry analysis of mitochondrial potential in $CD11b^+$, $CD45^+$ cells of 5xFAD HK2-haploinsufficient mice as described in (F) ($n = 3$ per group, unpaired t test).

(H) Co-localization analysis of HK2 and VDAC in the 5xFAD mice treated with LND. Representative confocal microscopy images showing HK2 (green) and VDAC (red) and their co-localization (white) in resting and activated microglia from mice treated with vehicle or LND.

(I) Pearson quantification shows that activated microglia display decreased levels of mitochondrial association, and LND treatment fails to recover this effect ($^{***}p < 0.001$, $^{****}p < 0.0001$, $n = 4$, >50 cells per group, one-way ANOVA, Tukey's posttest).

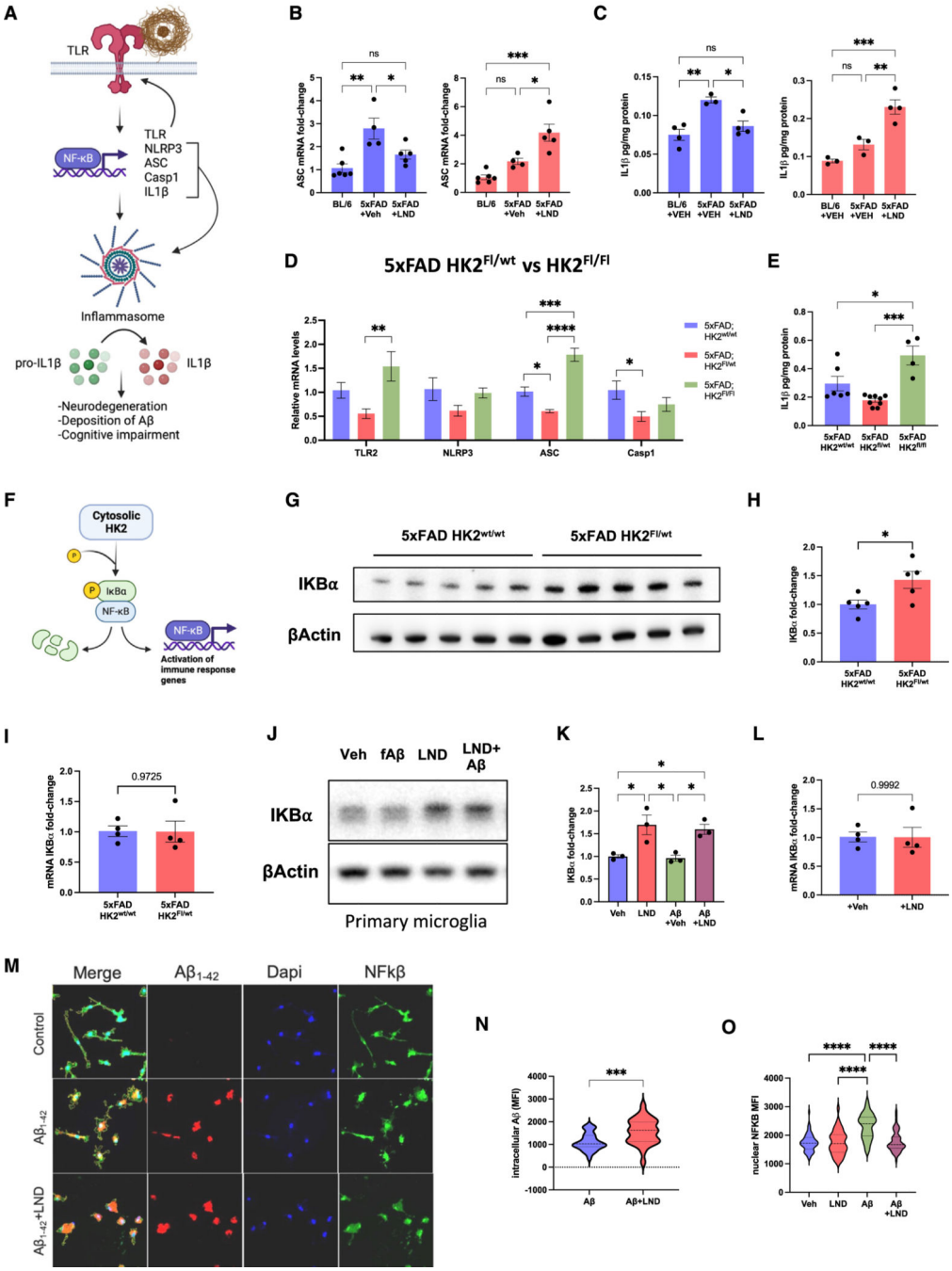

Figure 7. HK2 gene dosage induces opposite results in the induction of inflammation

(A) Schematic of the inflammasome pathway and the production of IL-1β.

(B) qPCR analysis of ASC in the cortex of male (blue graphs) and female (salmon graphs) BL/6 and 5xFAD mice treated with LND. *$p < 0.05$, **$p < 0.01$, ***$p < 0.001$ ($n = 4–6$ per group, one-way ANOVA, Tukey's posttest).

(C) ELISA of IL-1β levels in LND-treated 5-month-old 5xFAD male (blue graphs) and female (salmon graphs) mice (*$p < 0.05$, **$p < 0.01$; $n = 3–4$, one-way ANOVA, Tukey's posttest).

(D) qPCR analysis of inflammasome elements in 5xFAD mice with different HK2 gene dosages. *$p < 0.05$, **$p < 0.01$, ***$p < 0.001$, ****$p < 0.0001$ ($n = 4–5$ per group, one-way ANOVA, Tukey's posttest).

(E) ELISA of IL-1β levels in 5xFAD mice with different HK2 gene dosages. *$p < 0.05$, ***$p < 0.001$ ($n = 4–9$, one-way ANOVA, Tukey's posttest).

(F) Schematic of HK2 cytosolic regulation of NF-κB nuclear translocation mediated by its actions over IKBα protein degradation as described by Guo et al.[51]

(G–I) Expression levels of IKBα in the cortex of 5xFAD mice haploinsufficient for HK2 evaluated by qPCR (I, $n = 4$ per group, unpaired t test) and western blot (G and H, *$p < 0.05$, $n = 5$ per group, unpaired t test).

(J and K) Protein levels of IKBα evaluated by western blot in primary cultures of microglia treated with Aβ and LND (*$p < 0.05$, $n = 3$ per group, one-way ANOVA, Tukey's posttest).

(L) mRNA levels of IKBα evaluated by qPCR in primary cultures of microglia treated with LND (*$p < 0.05$, $n = 4$ per group, unpaired t test).

(M) Representative confocal microscopy images showing NF-κB (green) nuclear translocation (DAPI, blue) in primary cultures of microglia co-incubated with aggregated Aβ1–42 (red) and LND for 24 h.

(N and O) Quantification of intracellular Aβ and nuclear NF-κB mean fluorescence intensity as shown in (L). ***$p < 0.001$, ****$p < 0.0001$ ($n = 3$ coverslips from three independent cultures, unpaired t test and one-way ANOVA, Tukey's posttest, respectively).

KEY RESOURCES TABLE

REAGENT or RESOURCE	SOURCE	IDENTIFIER
Antibodies		
Recombinant Anti-Hexokinase 2 antibody	Abcam	Abcam Cat# ab209847; RRID: AB_2904621
AIF-1/Iba1 Antibody	Novus Biologicals	Novus Cat# NB100–1028; RRID: AB_521594
Anti-Hexokinase 1 antibody	Santa Cruz	Santa Cruz Biotechnology Cat# sc-46695; RRID: AB_627721
Anti-VDAC2 antibody	Abcam	Abcam Cat# ab37985; RRID: AB_778790
Anti-Trem2 antibody	R&D system	R&D system Cat# AF1729; RRID: AB_354956
Anti-beta Amyloid antibody [MOAB-2]	Abcam	Abcam Cat# ab126649; RRID: AB_3095985
Anti-IKB alpha Antibody [E130]	Abcam	Abcam Cat# ab32518; RRID: AB_733068
Anti-NF-kB p65 Antibody [E379]	Abcam	Abcam Cat# ab32536; RRID: AB_776751
Anti-NF-kB p65 (acetyl K310) Antibody	Abcam	Abcam Cat# ab19870; RRID: AB_776753
Anti-CD45 Antibody [MEM-28]	Novus Biologicals	Novus Cat# NB500–319; RRID: AB_10001403
Anti-CD11b Antibody [M1/70.15]	Novus Biologicals	Novus Cat# NB600–1327; RRID:AB_10001403
Anti-NeuN Antibody	Millipore	Millipore Cat# ABN90P; RRID: AB_2341095
Anti-Beta Actin Antibody	Santa Cruz	Santa Cruz Biotechnology Cat# sc-130065; RRID: AB_1249316
Anti-Lamp1 Antibody	R&D system	R&D system Cat# AF4320; RRID:AB_2296826
Chemicals, peptides, and recombinant proteins		
Lonidamine	Cayman Chemical Company	14640
Thiofavin S	Sigma-Aldrich	T1892
PLX5622	Plexxikon	AIN-7
Beta-Amyloid (1–42) Human	Anaspec Inc.	AS-2027
Tamoxifen, ≥99%	Sigma-Aldrich	T5648
(Z)-4-Hydroxytamoxifen, ≥98% Z isomer	Sigma-Aldrich	H7904
Methoxy X-04	Tocris Bioscience	4920
Dapi	Sigma-Aldrich	Cat. #D9542
Critical commercial assays		

REAGENT or RESOURCE	SOURCE	IDENTIFIER
Mitotracker Deep Red FM	Thermo Fisher Scientific	M22426
Hexokinase Activity Assay Kit (Fluorometric)	Abcam	ab211103
Luminescent ATP Detection Assay Kit	Abcam	ab113849
CellTiter 96® AQueous one solution Cell Proliferation Assay (MTS)	Promega	Cat#G3582
nCounter Glial profiling panel	Nanostring	1150000436
V-PLEX Proinflammatory Panel 1 Mouse Kit	Meso Scale Diagnostics	K15048D-1
Macs Neural tissue Dissociation kit	Miltenyl Biotec	130–092-628
BD Cytofix/cytoperm kit	BD Biosciences	Cat.# BDB554722
Deposited data		
Gene expression profiles of human prefrontal cortex brain tissues. Custom-made Agilent 44K array	Narayanan, et al.[60]	GSE33000
Experimental models: Cell lines		
Human microglia clone 3 (HMC3) cells	ATCC	CRL-3304
Experimental models: Organisms/strains		
C57BL/6J mice	Bred in-house (From: Jackson Laboratory)	000664
5xFAD mice	Bred in-house (From: Jackson Laboratory)	034848
HK2 Fl/Fl mice	Nissim Hay Lab [31]	N/A
Cx3cr1CreER knockin/knockout mice	Bred in-house (From: Jackson Laboratory)	020940
5xFAD: CX3CR1-creERT2:HK2Fl/wt	This paper	N/A
5xFAD: CX3CR1-creERT2:HK2Fl/Fl mice	This paper	N/A
5xFAD: CX3CR1-creERT2:HK2wt/wt	This paper	N/A
Oligonucleotides		
Mouse HK2 TaqMan probe	Thermo Fisher Scientific	Mm00443385_m1
Human HK2 Taqman probe	Thermo Fisher Scientific	Hs00606086_m1
Mouse HK1 Taqman probe	Thermo Fisher Scientific	Mm00439344_m1
Mouse HK3 Taqman probe	Thermo Fisher Scientific	Mm01341942_m1
Mouse CD36 Taqman probe	Thermo Fisher Scientific	Mm00432403_m1

REAGENT or RESOURCE	SOURCE	IDENTIFIER
Mouse APOE Taqman probe	Thermo Fisher Scientific	Mm00437573_m1
Mouse FABP5 Taqman probe	Thermo Fisher Scientific	Mm00783731_s1
Mouse IL6 Taqman probe	Thermo Fisher Scientific	Mm00446190_m1
Mouse TNF Taqman probe	Thermo Fisher Scientific	Mm00443258_m1
Mouse Spp1 Taqman probe	Thermo Fisher Scientific	Mm00436767_m1
Mouse Axl Taqman probe	Thermo Fisher Scientific	Mm00437221_m1
Mouse Mertk Taqman probe	Thermo Fisher Scientific	Mm00434920_m1
Mouse TGFB1 Taqman probe	Thermo Fisher Scientific	Mm01178820_m1
Mouse TGFBR1 Taqman probe	Thermo Fisher Scientific	Mm00436964_m1
Mouse ASC taqman probe	Thermo Fisher Scientific	Mm00445747_g1
Mouse Trem2 taqman probe	Thermo Fisher Scientific	Mm04209422_m1
Mouse Clec7a taqman probe	Thermo Fisher Scientific	Mm01183349_m1
Mouse LPL taqman probe	Thermo Fisher Scientific	Mm00434764_m1
Mouse Ikba taqman probe	Thermo Fisher Scientific	Mm00477798_m1
Mouse TLR2 taqman probe	Thermo Fisher Scientific	Mm00442346_m1
Mouse NLRP3 taqman probe	Thermo Fisher Scientific	Mm00840904_m1
Mouse Casp1 taqman probe	Thermo Fisher Scientific	Mm01226172_m1
Mouse C1qa taqman probe	Thermo Fisher Scientific	Mm07295529_m1
Mouse C1qb taqman probe	Thermo Fisher Scientific	Mm01179619
Mouse C1qc taqman probe	Thermo Fisher Scientific	Mm00776126_m1
Mouse C3 taqman probe	Thermo Fisher Scientific	Mm01232779_m1
Mouse IL1β taqman probe	Thermo Fisher Scientific	Mm01336189
Mouse Tyrobp taqman probe	Thermo Fisher Scientific	Mm00449152_m1
Mouse GAPD (GAPDH) Endogenous Control	Thermo Fisher Scientific	4352339E
Human GAPD (GAPDH) Endogenous Control	Thermo Fisher Scientific	4333764F
Software and algorithms		
FlowJo 10.10	BD Biosciences	https://www.flowjo.com
Prism 10.0	GraphPad	https://www.graphpad.com/
FIJI-ImageJ	NIH	https://fiji.sc
Rosalind Analysis Platform	OnRamp Bioinformatics	https://www.rosalind.bio

REAGENT or RESOURCE	SOURCE	IDENTIFIER
Agora	AMP-AD consortium	https://agora.adknowledgeportal.org
Other		
Western Blotting Detection Reagent	GE healthcare	Cat#RPN2235
BD Fortessa	BD Biosciences	N/A
Amersham imager 600	GE healthcare	N/A